Article

Key Science Goals for the Next-Generation Event Horizon Telescope

Michael D. Johnson [1,2,*], Kazunori Akiyama [2,3,4], Lindy Blackburn [1,2], Katherine L. Bouman [5], Avery E. Broderick [6,7,8], Vitor Cardoso [9,10], Rob P. Fender [11,12], Christian M. Fromm [13,14,15], Peter Galison [2,16,17], José L. Gómez [18], Daryl Haggard [19,20], Matthew L. Lister [21], Andrei P. Lobanov [15], Sera Markoff [22,23], Ramesh Narayan [1,2], Priyamvada Natarajan [2,24,25], Tiffany Nichols [26], Dominic W. Pesce [1,2], Ziri Younsi [27], Andrew Chael [28], Koushik Chatterjee [1,2], Ryan Chaves [1], Juliusz Doboszewski [2,29], Richard Dodson [30], Sheperd S. Doeleman [1,2], Jamee Elder [2,29], Garret Fitzpatrick [1], Kari Haworth [1], Janice Houston [1], Sara Issaoun [1,†], Yuri Y. Kovalev [15,31,32], Aviad Levis [5], Rocco Lico [18,33], Alexandru Marcoci [34], Niels C. M. Martens [29,35,36], Neil M. Nagar [37], Aaron Oppenheimer [1], Daniel C. M. Palumbo [1,2], Angelo Ricarte [1,2], María J. Rioja [30,38,39], Freek Roelofs [1,2,40], Ann C. Thresher [41], Paul Tiede [1,2], Jonathan Weintroub [1,2] and Maciek Wielgus [15]

1   Center for Astrophysics | Harvard & Smithsonian, 60 Garden Street, Cambridge, MA 02138, USA
2   Black Hole Initiative, Harvard University, 20 Garden Street, Cambridge, MA 02138, USA
3   Massachusetts Institute of Technology Haystack Observatory, 99 Millstone Road, Westford, MA 01886, USA
4   National Astronomical Observatory of Japan, 2-21-1 Osawa, Mitaka, Tokyo 181-8588, Japan
5   California Institute of Technology, 1200 East California Boulevard, Pasadena, CA 91125, USA
6   Perimeter Institute for Theoretical Physics, 31 Caroline Street North, Waterloo, ON N2L 2Y5, Canada
7   Department of Physics and Astronomy, University of Waterloo, 200 University Avenue West, Waterloo, ON N2L 3G1, Canada
8   Waterloo Centre for Astrophysics, University of Waterloo, Waterloo, ON N2L 3G1, Canada
9   Niels Bohr International Academy, Niels Bohr Institute, Blegdamsvej 17, 2100 Copenhagen, Denmark
10 CENTRA, Departamento de Física, Faculdade de Ciências, Instituto Superior Técnico—IST, Universidade de Lisboa, Campo Grande, 1749-016 Lisboa, Portugal
11 Astrophysics, Department of Physics, University of Oxford, Keble Road, Oxford OX1 3RH, UK
12 Department of Astronomy, University of Cape Town, Private Bag X3, Rondebosch 7701, South Africa
13 Institut für Theoretische Physik und Astrophysik, Universität Würzburg, Emil-Fischer-Strasse 31, D-97074 Würzburg, Germany
14 Institut für Theoretische Physik, Goethe Universität, Max-von-Laue-Str. 1, D-60438 Frankfurt, Germany
15 Max-Planck-Institut für Radioastronomie, Auf dem Hügel 69, D-53121 Bonn, Germany
16 Department of History of Science, Harvard University, Cambridge, MA 02138, USA
17 Department of Physics, Harvard University, Cambridge, MA 02138, USA
18 Instituto de Astrofísica de Andalucía-CSIC, Glorieta de la Astronomía s/n, E-18008 Granada, Spain
19 Department of Physics, McGill University, 3600 rue University, Montreal, QC H3A 2T8, Canada
20 Trottier Space Institute at McGill, 3550 rue University, Montreal, QC H3A 2A7, Canada
21 Department of Physics and Astronomy, Purdue University, 525 Northwestern Avenue, West Lafayette, IN 47907, USA
22 Anton Pannekoek Institute for Astronomy, University of Amsterdam, Science Park 904, 1098 XH Amsterdam, The Netherlands
23 Gravitation and Astroparticle Physics Amsterdam (GRAPPA) Institute, University of Amsterdam, Science Park 904, 1098 XH Amsterdam, The Netherlands
24 Department of Astronomy, Yale University, 52 Hillhouse Avenue, New Haven, CT 06511, USA
25 Department of Physics, Yale University, P.O. Box 208121, New Haven, CT 06520, USA
26 Department of History, Princeton University, Dickinson Hall, Princeton, NJ 08544, USA
27 Mullard Space Science Laboratory, University College London, Holmbury St. Mary, Dorking, Surrey RH5 6NT, UK
28 Princeton Gravity Initiative, Princeton University, Jadwin Hall, Princeton, NJ 08544, USA
29 Lichtenberg Group for History and Philosophy of Physics, University of Bonn, 53113 Bonn, Germany
30 ICRAR, M468, The University of Western Australia, 35 Stirling Hwy, Crawley, WA 6009, Australia
31 Lebedev Physical Institute of the Russian Academy of Sciences, Leninsky prospekt 53, 119991 Moscow, Russia
32 Moscow Institute of Physics and Technology, Institutsky per. 9, 141700 Dolgoprudny, Russia
33 INAF-Istituto di Radioastronomia, Via P. Gobetti 101, I-40129 Bologna, Italy
34 Centre for the Study of Existential Risk, University of Cambridge, 16 Mill Lane, Cambridge CB2 1SB, UK
35 Freudenthal Institute, Utrecht University, 3584 CC Utrecht, The Netherlands

[36] Descartes Centre for the History and Philosophy of the Sciences and the Humanities, Utrecht University, 3584 CC Utrecht, The Netherlands

[37] Astronomy Department, Universidad de Concepción, Casilla 160-C, Concepción 4030000, Chile

[38] CSIRO Astronomy and Space Science, PO Box 1130, Bentley, WA 6102, Australia

[39] Observatorio Astronómico Nacional (IGN), Alfonso XII, 3 y 5, 28014 Madrid, Spain

[40] Department of Astrophysics, Institute for Mathematics, Astrophysics and Particle Physics (IMAPP), Radboud University, P.O. Box 9010, 6500 GL Nijmegen, The Netherlands

[41] McCoy Family Center for Ethics, Stanford University, Stanford, CA 94305, USA

* Correspondence: mjohnson@cfa.harvard.edu

† NASA Hubble Fellowship Program, Einstein Fellow.

Abstract: The Event Horizon Telescope (EHT) has led to the first images of a supermassive black hole, revealing the central compact objects in the elliptical galaxy M87 and the Milky Way. Proposed upgrades to this array through the next-generation EHT (ngEHT) program would sharply improve the angular resolution, dynamic range, and temporal coverage of the existing EHT observations. These improvements will uniquely enable a wealth of transformative new discoveries related to black hole science, extending from event-horizon-scale studies of strong gravity to studies of explosive transients to the cosmological growth and influence of supermassive black holes. Here, we present the key science goals for the ngEHT and their associated instrument requirements, both of which have been formulated through a multi-year international effort involving hundreds of scientists worldwide.

Keywords: black holes; general relativity; interferometry; accretion; relativistic jets; very-long-baseline interferometry; EHT; ngEHT

1. Introduction

The Event Horizon Telescope (EHT) has produced the first images of the supermassive black holes (SMBHs) in the M87 galaxy ([1–8], hereafter M87* I–VIII) and at the center of the Milky Way ([9–14], hereafter Sgr A* I–VI). Interpretation of the EHT results for Sgr A* and M87* has relied heavily upon coordinated multi-wavelength campaigns spanning radio to gamma-rays ([10], ETH MWL Science Working Group et al. [15]) In addition, the EHT has made the highest resolution images to date of the inner jets of several nearby Active Galactic Nuclei (AGN), demonstrating the promise of millimeter VLBI in making major contributions to the studies of relativistic radio jets launched from SMBHs (Kim et al. [16], Janssen et al. [17], Issaoun et al. [18], Jorstad et al. [19]).

The EHT results were achieved using the technique of very-long-baseline interferometry (VLBI). In this approach, radio signals are digitized and recorded at a collection of telescopes; the correlation function between every pair of telescopes is later computed offline, with each correlation coefficient sampling one Fourier component of the sky image with angular frequency given by the dimensionless vector baseline (measured in wavelengths) projected orthogonally to the line of sight [20]. The EHT observations at 230 GHz are the culmination of pushing VLBI to successively higher frequencies across decades of development (e.g., [21–23]), giving a diffraction-limited angular resolution of $\sim$20 µas (for a review of mm-VLBI, see [24]). For comparison, the angular diameter of the lensed event horizon—the BH "shadow"—is $\theta_{\rm sh} \approx 10GM/(c^2D)$, where G is the gravitational constant, c is the speed of light, M is the BH mass, and D is the BH distance [25–28]. For M87*, $\theta_{\rm sh} \approx 40$ µas; for Sgr A*, $\theta_{\rm sh} \approx 50$ µas.

Despite the remarkable discoveries of the EHT, they represent only the first glimpse of the promise of horizon-scale imaging studies of BHs and of high-frequency VLBI more broadly. In particular, the accessible science in published EHT results is severely restricted in several respects:

- EHT images are effectively monochromatic. The currently published EHT measurements sample only 4 GHz of bandwidth, centered on 228 GHz. BH images are expected to have a complex structure in frequency, with changing synchrotron emissivity, opti-

cal depth, and Faraday effects, making multi-frequency studies a powerful source of physical insight (see, e.g., [29–32]). The EHT has successfully completed commissioning observations at 345 GHz [33], which is now a standard observing mode. However, 345 GHz observations will be strongly affected by atmospheric absorption, severely affecting sensitivity and likely restricting detections to intermediate baseline lengths among the most sensitive sites (e.g., [34]).

- EHT images have severely limited image dynamic range. Current EHT images are limited to a dynamic range of only ~10 [4,11], providing only modest information about image signatures that are related to the horizon and limiting the ability to connect the event-horizon-scale images to their relativistic jets seen until now only at larger scales, via lower wavelength observations.[1]

  For comparison, VLBI arrays operating at centimeter wavelengths routinely achieve a dynamic range of ~10^4 on targets such as M87* (e.g., [35]).

- EHT observations have only marginally resolved the rings in Sgr A* and M87*. The EHT only samples a few resolution elements across the images. For instance, the EHT has only determined an upper limit on the thickness of the M87* ring [6], and the azimuthal structure of the rings in both sources is poorly constrained.

- EHT images cannot yet study the dynamics of M87* or Sgr A*. The gravitational timescale is $t_g \equiv GM/c^3 \approx 9$ h for M87* and is $t_g \approx 20$ s for Sgr A*. In each source, the expected evolution timescale is ~$50\, t_g$ (e.g., [36])—approximately 20 days for M87* and 20 min for Sgr A*. Current EHT campaigns consist of sequential observing nights extending for only ~1 week, which is too short to study the dynamical evolution of M87*. Moreover, the current EHT baseline coverage is inadequate to meaningfully constrain the rapid dynamical evolution of Sgr A*, which renders standard Earth-rotation synthesis imaging inapplicable [11,12].

In short, published EHT images of M87* and Sgr A* currently sample only 5×5 spatial resolution elements, a single spectral resolution element, and a single temporal resolution element (snapshot for M87*; time-averaged for Sgr A*).

The next-generation EHT (ngEHT) is a project to design and build a significantly enhanced EHT array through the upgrade, integration, or deployment of additional stations (e.g., [37–44]), the use of simultaneous observations at three observing frequencies [45–47], and observations that extend over several months or more with a dense coverage in time [48]. The ngEHT currently envisions two primary development phases. In Phase 1, the ngEHT will add three or more dedicated telescopes to the current EHT, with primarily dual-band (230/345 GHz) observations over ~3 months per year.[2] In Phase 2, the ngEHT will add five or more additional dedicated telescopes, with simultaneous tri-band capabilities (86/230/345 GHz) at most sites and observations available year-round. The new ngEHT antennas are expected to have relatively modest diameters (6–10 m), relying on wide recorded bandwidths, strong baselines to large existing apertures, and long integrations enabled through simultaneous multi-band observations to achieve the needed baseline sensitivity. Figure 1 shows candidate ngEHT sites in each phase.

These developments will sharply improve upon the performance of the EHT. Relative to other premier and planned facilities that target high-resolution imaging (such as the SKA, ngVLA, ALMA, and ELTs), the defining advantage of the EHT is its unmatched angular resolution. However, relative to the imaging capabilities of the current EHT, the defining improvements of the ngEHT images will be in accessing *larger* angular scales through the addition of *shorter* interferometric baselines than those of the present array, and in expanding the simultaneous frequency coverage. In addition, the ngEHT will extend accessible timescales of the current EHT by ~5 orders of magnitude, enabling dynamic analysis with the creation of movies of Sgr A* (through improved "snapshot" imaging on ~minute timescales) and AGN including M87* (through densely sampled monitoring campaigns that extend from months to years). Figures 2 and 3 summarize these improvements.
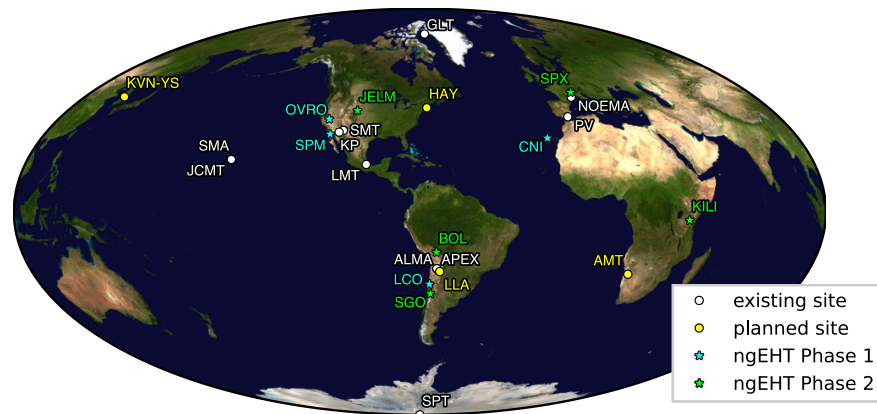
Figure 1. Distribution of EHT and ngEHT sites around the globe. Sites that have joined EHT campaigns are shown in white (see [2]), additional ngEHT Phase-1 sites are shown in cyan, and ngEHT Phase-2 sites are shown in green. Three of the EHT sites have joined since its initial observing campaign in 2017: the 12 m Greenland Telescope (GLT; [49]), the 12 m Kitt Peak Telescope (KP), the Northern Extended Millimeter Array (NOEMA) composed of twelve 15 m dishes. Several other existing or upcoming sites that plan to join EHT/ngEHT observations are shown in yellow: the 37 m Haystack Telescope (HAY; [41]), the 21 m Yonsei Radio Observatory of the Korea VLBI Network (KVN-YS; [42]), the 15 m Africa Millimetre Telescope (AMT; [43]), and the 12 m Large Latin American Millimeter Array (LLA; [44]). For additional details on the planned ngEHT specifications, see ngEHT Collaboration [50].
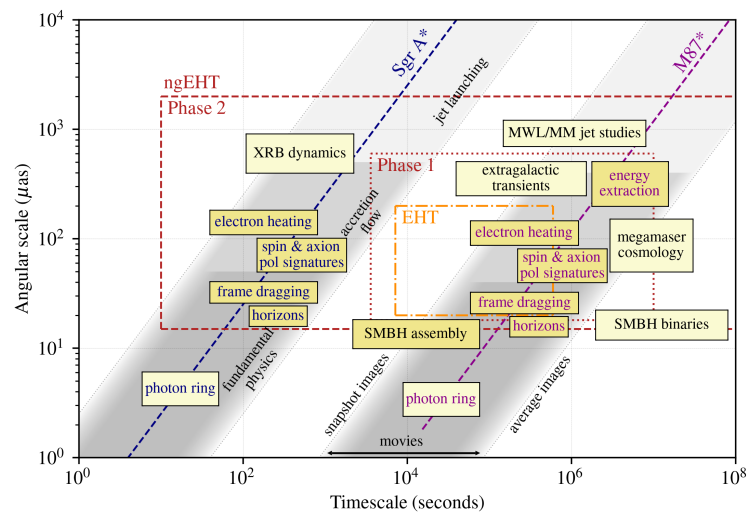
Figure 2. Comparison of image angular resolutions and timescales accessible to the EHT and ngEHT and the associated scientific opportunities. For M87* and Sgr A*, the ranges of angular resolution and timescale needed to study the three primary domains–fundamental physics, accretion, and jet launching–are indicated with the tilted shaded regions. These shaded regions are centered on the resolution-timescale for each source determined by the speed of light ($ct = D\theta$). Snapshot images require an array to form images on these timescales or shorter; average images require an array to form images over significantly longer timescales; movies require that an array can form images of the full range of timescales from snapshots to averages. The primary difference in M87* and Sgr A* is the factor of ~1500 difference in the SMBH mass, which sets the system timescale. In contrast, the relevant angular scales in these systems are determined by the mass-to-distance ratio, which only differs by ~20% for these two SMBHs. The approximate resolution-timescale pair to study each of the ngEHT Key Science Goals is indicated with the inset labeled boxes. Goals associated with Sgr A* or M87* are colored in blue or purple, respectively.
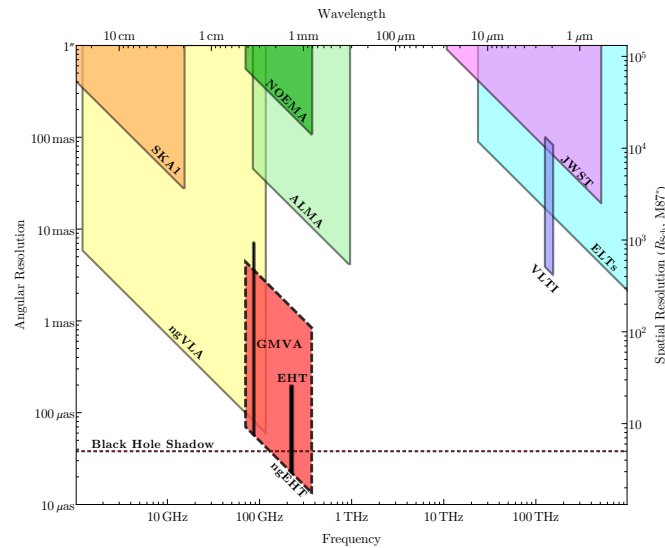
Figure 3. Range of observing frequency and angular resolution for selected current and upcoming facilities, from radio to the infrared. The ngEHT can achieve an imaging angular resolution that is significantly finer than any other planned facility or experiment. The ngEHT also envisions simultaneous multi-band observations, extending from 86 to 345 GHz, which will significantly expand the frequency coverage of currently published EHT data (black filled region). Figure adapted from Selina et al. [51].

To guide its design, the ngEHT has developed a set of Key Science Goals over the past two years, with contributions from hundreds of scientists. This process has included three international meetings[3,4,5], a Science Requirements Review (focused on identifying the most significant ngEHT science drivers), and a System Requirements Review (focused on identifying the associated instrument requirements). In addition, the ngEHT project has convened focused workshops on major topics, including assessing the motivation for adding 86 GHz capabilities to the ngEHT design to leverage phase transfer techniques[6], environmental and cultural issues related to ethical telescope siting, and the role of History, Philosophy, and Culture in the ngEHT (see Section 2.8 and [52] hereafter HPC White Paper). A series of papers present many aspects of these science cases in greater depth in a special issue of *Galaxies*[7].

In this paper, we summarize the Key Science Goals of the ngEHT and associated instrument requirements. We begin by discussing specific scientific objectives, organized by theme, in Section 2. We then summarize the prioritization and aggregated requirements of these science cases together with a condensed version of the ngEHT Science Traceability Matrix (STM) in Section 3. Details on the ngEHT concept, design, and architecture are presented in a companion paper [50].

2. Key Science Goals of the ngEHT

The ngEHT Key Science Goals were developed across eight Science Working Groups (SWGs). These goals span a broad range of targets, spatial scales, and angular resolutions (see Figure 2). We now summarize the primary recommendations from each of these working groups: Fundamental Physics (Section 2.1), Black Holes and their Cosmic Context (Section 2.2), Accretion (Section 2.3), Jet Launching (Section 2.4), Transients (Section 2.5), New Horizons (Section 2.6), Algorithms and Inference (Section 2.7), and History, Philosophy, and Culture (Section 2.8).

2.1. Fundamental Physics

BHs are an extraordinary prediction of general relativity: the most generic and simple macroscopic objects in the Universe. Among astronomical targets, BHs are unique in their ability to convert energy into electromagnetic and gravitational radiation with remarkable

efficiency (e.g., [53–56]). Meanwhile, the study of BH stability and dynamics challenges our knowledge of partial differential equations, of numerical methods, and of the interplay between quantum field theory and the geometry of spacetime. The BH information paradox (e.g., [57]) and the existence of unresolved singularities in classical general relativity (e.g., [53,58]) point to deep inconsistencies in our current understanding of gravity and quantum mechanics. It is becoming clear that the main conceptual problems in BH physics hold the key to many current open foundational issues in theoretical physics.

Astrophysical BH systems are therefore an extraordinary test-bed for fundamental physics, although their extreme compactness renders them observationally elusive. Matter moving in the vicinity of an event horizon is subject to both extreme (thermo)dynamical conditions and intense gravitational fields, thereby providing a unique laboratory for the study of physical processes and phenomena mediated by the strongest gravitational fields in the Universe. Furthermore, by understanding the properties of matter and polarised electromagnetic radiation in this highly-nonlinear (and dynamical) regime, we can probe the underlying spacetime geometry of BHs and perform new tests of general relativity. The key to studying physics near the horizon is the capability to resolve, accurately extract, and precisely measure different features in BH images (see Figure 4). These image features can be periodic (e.g., oscillating fields), transient (e.g., reconnective processes and flares), persistent (the photon ring), or stochastic about a mean (e.g., polarization spiral patterns).
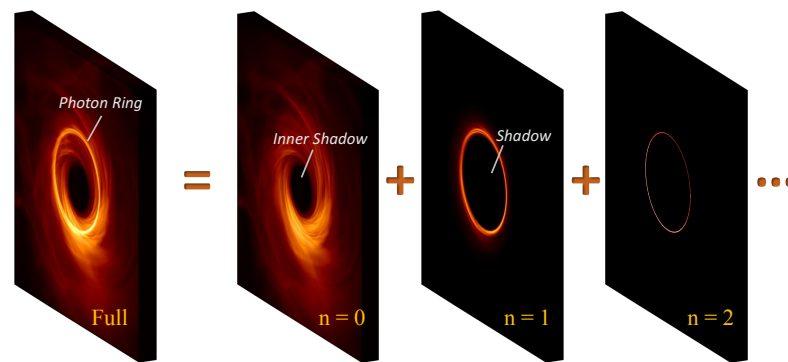
Figure 4. BH images display a series of distinctive relativistic features such as the BH apparent "shadow" (e.g., [27]), "inner shadow" (e.g., [59]), and "photon ring" (e.g., [60]).

The previous measurements of M87* and Sgr A* from the EHT provide compelling evidence for supermassive compact objects. The ngEHT has the capability to elevate existing EHT probes of the strong-field regime. We now describe four key science goals that target foundational topics in fundamental physics: studies of horizons (Section 2.1.1), measurements of SMBH spin (Section 2.1.2), studies of a BH photon ring (Section 2.1.3), and constraints on ultralight boson fields (Section 2.1.4). For a comprehensive discussion of these topics, see ngEHT Fundamental Physics SWG et al. [61].

2.1.1. Existence and Properties of Horizons

The formation of horizons (regions of spacetime that trap light) as gravitational collapse unfolds is one of the main and outstanding predictions of classical general relativity. Robust singularity theorems assert that BH interiors are also regions of breakdown of the classical Einstein equations, while quantum field theory is still associated with conundrums in the presence of horizons. Testing the existence and properties of horizons is therefore a key strong-field test of general relativity [62,63]. In astronomical terms, a horizon would be characterised by a complete absence of emission. It is clear that quantitative discussions of horizon physics will be strongly influenced both by the error in observational images and the modelling of matter and (spacetime) geometry at the core of simulated images.

For example, many models, especially those with spherical accretion onto BHs, tend to exhibit a pronounced apparent "shadow" (e.g., [27,64–66]). This feature shows a sharp

brightness gradient at the boundary of the "critical curve" that corresponds to the boundary of the observer's line of sight into the BH. In contrast, models in which the emission is confined to a thin disk that extends to the horizon show a sharp brightness gradient in a smaller feature, the "inner shadow", which corresponds to the direct lensed image of the equatorial horizon [26,59,67]. The inner shadow gives the observer's line of sight into the BH that is unobscured by the equatorial emitting region.

Hence, BHs can give rise to a rich array of distinctive image features, but studies of horizons through imaging must account for potential degeneracies between the properties of the spacetime and those of the emitting material. Firm conclusions from imaging with the ngEHT will require significant improvements in both the image dynamic range and angular resolution of current EHT images, which have primarily demonstrated consistency with predictions of the Kerr metric (see Figure 5) and order-unity constraints on potential violations of general relativity (see, e.g., Sgr A* VI [14], Psaltis et al. [68], Kocherlakota et al. [69]). To leading order, the image dynamic range of the ngEHT will determine the luminosity of the features that can be studied, while the angular resolution will determine the size of the features that can be studied. Hence, quantitative statements about the existence of horizons will be primarily influenced by the dynamic range that can be achieved, while quantitative properties of the spacetime will be determined by the angular resolution [70,71]. Figure 6 shows an example of the improvement in both quantities that is possible using the ngEHT, enabling new studies of image signatures of the horizon. For additional discussion of potential ngEHT constraints on exotic horizonless spacetimes such as naked singularities and (non-hidden) wormholes, see ngEHT Fundamental Physics SWG et al. [61]. In addition to the necessity of image improvements, multi-frequency studies will be imperative to securely disentangle properties of the emission (which are chromatic) from features associated with the lensed horizon (which is achromatic). For all studies of horizons through imaging with the ngEHT, M87* and Sgr A* will be the primary targets because of their large angular sizes.
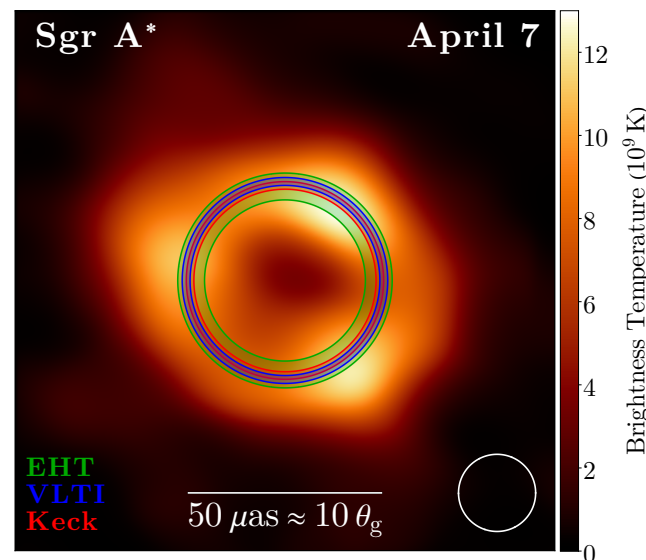
Figure 5. EHT representative average image of Sgr A* using data from 7 April 2017 [11]. The white circle in the lower-right shows a 20 µas beam that gives the approximate EHT resolution. The overlaid annuli show the predicted ranges of the Sgr A* critical curve using measurements of resolved stellar orbits using the VLTI (blue; [72]) and Keck (red; [73]); the ranges are dominated by the potential variation in size with spin, $d_{sh} = (9.6$–$10.4)\theta_g$ [25,74]. The green annulus shows the estimated range ($\pm 1\sigma$) of the critical curve using EHT measurements, which is consistent with these predictions [14]. However, because of the limited baseline coverage of the EHT, key image features such as the azimuthal brightness around the ring and the depth and shape of the central brightness depression are only weakly constrained with current observations.
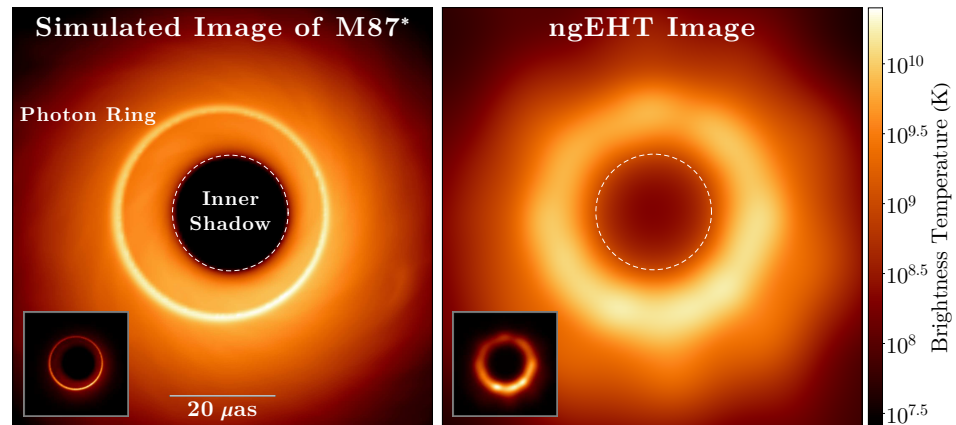
Figure 6. Accessing signatures of the event horizon with the ngEHT. Each panel shows an image on a logarithmic scale, with an inset shown with a linear scale. The left panel shows a time-averaged simulated image of M87*, which shows a prominent photon ring and inner shadow. The right panel shows a reconstructed ngEHT image using the Bayesian VLBI analysis package `Comrade.jl` [75] applied to simulated ngEHT phase-1 observations. The ngEHT provides both the angular resolution and dynamic range required to identify the deep brightness depression produced by the inner shadow in this simulated image.

2.1.2. Measuring the Spin of a SMBH

Astrophysical BHs are expected to be completely characterized by their mass and angular momentum [55,76,77]. Estimates of a SMBH spin through direct imaging would provide an invaluable complement to other techniques, such as the X-ray reflection method (see, e.g., [78]). However, the current EHT measurements provide only marginal, model-dependent constraints on the spins of M87* and Sgr A* [5,8,13].

The ngEHT has the opportunity to provide decisive measurements of spin through several approaches (for a summary of these methods, see [79]). The most compelling method would be to study the detailed structure of the lensing signatures such as the photon ring (see Section 2.1.3), or the (inner) shadow (see Section 2.1.1). However, while spin has a pronounced effect on these features, the effects of spin manifest on scales that are still much smaller than the nominal resolution of the ngEHT, so a conclusive detection may not be possible. Nevertheless, the effects of spin may be apparent in the emission structure on somewhat larger scales, particularly through the polarization structure in the emission ring (see Figure 7 and [80,81]). Finally, spin signatures are expected to be imprinted in the time-domain.

At least initially, ngEHT estimates of spin will likely rely on numerical simulations because unambiguous signatures of spin would require significantly finer angular resolution. These estimates will likely require confirmation through multiple lines of study—total intensity, polarization, and time-domain—and through a variety of modeling approaches including semi-analytic studies (e.g., [82]). Current studies indicate that the time-averaged polarized structure of M87* is the most reliable estimator of spin, with 345 GHz observations essential to improving angular resolution and also to quantify the potential effects of internal Faraday rotation on the polarized structure (see, e.g., [29,30,32]).
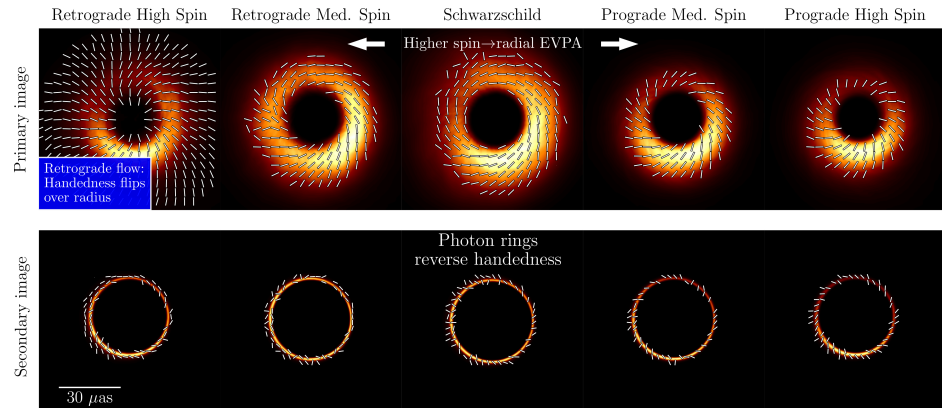
Figure 7. Summary of spin signatures in polarized images of time-averaged GRMHD simulations. In each panel, color indicates brightness and ticks show linear polarization direction. Rows show time-averaged primary (**top**) and secondary (**bottom**) images from MAD GRMHD simulations of M87*; columns show varying BH spin, ranging from a rapidly spinning BH with a retrograde accretion flow (**left**) to a non-spinning BH (**center**) to a rapidly spinning BH with a prograde accretion flow (**right**). The angular radius of the black hole, M/D, is identical in each panel. The polarization pattern becomes more radial at higher spin, as frame dragging enforces toroidal magnetic fields near the horizon. In retrograde flows, the spirals pattern reverses handedness over radius, indicating the transition from the prograde rotation within the ergosphere to the retrograde flow at larger radii. The handedness flips across sub-images, leading to depolarization in the photon ring of the full image (see [83,84]). By studying the polarized structure and its radial evolution, the ngEHT can estimate the spin of M87* and Sgr A* and quantify the effects of frame dragging. Adapted from Palumbo [85].

2.1.3. Constraining the Properties of a Black Hole's Photon Ring

The image of a BH is determined by two different factors: the complex astrophysical phenomena in its vicinity, which are the source of the emergent electromagnetic radiation, and the spacetime geometry, which introduces effects such as gravitational lensing and redshift. To isolate relativistic effects requires disentangling the complex, turbulent astrophysical environment from the comparatively simple spacetime dependence. Gravitational lensing is particularly useful in this context, as it gives rise to matter-independent ("universal") features, such as the "photon ring." The photon ring is a brightness enhancement along an approximately circular closed curve on the image, which arises from light rays undergoing multiple half-orbits around the BH before reaching the telescope [60]. These rays are small deviations from the unstable bound spherical orbits near a Kerr BH [25,86]. We index these half-orbits with the number n; the observer sees exponentially demagnified images of the accretion flow with each successive n (see Figure 4). At the resolution of Earth baselines at 230 GHz and 345 GHz, only $n = 0$ and $n = 1$ emission is likely to be detectable. Because the ngEHT cannot resolve the thickness of the primary ($n = 0$) ring, ngEHT studies of the photon ring necessarily require some degree of super-resolution, with associated model-dependent assumptions. In general, the principal challenge for ngEHT studies of the photon ring is to unambiguously disentangle the signals of the primary and secondary photon rings (see, e.g., [87]).

In the asymptotic ($n \to \infty$) limit, the photon ring has an intricate and universal structure which depends only on the spacetime geometry and acts as a lens for electromagnetic radiation (e.g., [74,88]). However, even at small-n, the photon ring carries information on the BH's mass and spin and provides a novel strong-field test of general relativity [89,90], especially if combined with a strong independent mass measurement (e.g., as is given by resolved stellar orbits of Sgr A*; see Figure 5). A clear goal for the ngEHT is to use the improved angular resolution and sensitivity to constrain the properties of the photon rings in M87* and Sgr A*.

Tests with both geometric model fitting of the sky intensity distribution and emissivity modelling in the BH spacetime suggest that the long baselines at 345 GHz are a strict requirement for detecting the $n = 1$ ring [82,87]. While intermediate baselines are required to support these model-fitting approaches, achieving the highest possible angular resolution is the driving requirement for studies of the photon ring. Photon ring detection using time-averaged images is likely most relevant to M87*, as Sgr A* observations are expected to be severely affected by scattering in the ionized interstellar medium [91–94]. Alternatively, signatures of the photon ring may be accessible in the time-domain, where "light echoes" can appear from either impulsive events such as flaring "hot spots" or from stochastic fluctuations in the accretion flow (see, e.g., [95–105]).

2.1.4. Constraining Ultralight Fields

The existence of ultralight boson fields with masses below the eV scale has been predicted by a plethora of beyond-Standard-Model theories (e.g., [106–110]). Such particles are compelling dark matter candidates and are, in general, extremely hard to detect or exclude with usual particle detectors. However, quite remarkably, rotating BHs can become unstable against the production of light bosonic particles through a process known as BH superradiance [111]. This process drives an exponential growth of the field in the BH exterior, while spinning the BH down. Superradiance is most effective for highly spinning BHs and when the boson's Compton wavelength is comparable to the BH's gravitational radius [111]. A BH of mass $\sim 10^{10} M_\odot$ such as M87* can be superradiantly unstable for ultralight bosons of masses 10^{-21} eV (this particular value leads to "fuzzy" dark matter, predicting a flat distribution that is favored by some observations; [112]).

For very weakly interacting particles, the process depends primarily on the mass and spin of the BH, and on the mass and spin of the fundamental boson. By requiring the predicted instability timescale to be smaller than the typical accretion timescale (that tends to spin up the BH instead), one can then draw regions in the parameter space where highly spinning BHs should not reside, if bosons within the appropriate mass range exists in nature. Thus, BH spin measurement can be used to constrain the existence of ultralight bosons. In particular, obtaining a lower limit on the BH spin is enough to place some constraints on boson masses (with the specific boson mass range constraint dependent on the BH spin). This approach is practically the only means to constrain weakly interacting fundamental fields in this mass range. Davoudiasl and Denton [113] used this line of argument to constrain masses of ultralight boson dark matter candidates with the initially reported EHT measurements that the SMBH must be spinning to produce sufficient jet power [5].

Among all the families of suggested ultralight particles, axions are one of the best studied and most highly motivated from a particle physics perspective. For axions with strong self-interactions, the super-radiance process will end up with a weakly saturating phase where the axion field saturates the highest possible density in the Universe. Due to the axion-photon coupling, the coherently oscillating axion field that forms around the BH due to superradiance can give rise to periodic rotation of the electric vector position angle (EVPA) of the linearly polarized emission. The amplitude of the EVPA oscillation is proportional to the axion-photon coupling constant and is independent of the photon frequency. The variations of the EVPA behave as a propagating wave along the photon ring for a nearly face-on BH. For instance, using the 4 days of polarimetric measurements of M87* published by the EHT collaboration in 2021 [7], one can already constrain the axion-photon coupling to previously unexplored regions [114,115]. The upper bound on the axion mass window is determined by the spin of the BH via the condition for superradiance to occur.

For improved constraints on these fundamental fields and their electromagnetic couplings, the ngEHT must observe polarimetric images of M87* in a series of at least 3 days over a 20-day window (the expected oscillation period). As for other cases that rely on polarimetry, observations at both 230 and 345 GHz are imperative to isolate the potential

effects of Faraday rotation, and repeated observations will be needed to distinguish periodic oscillations from stochastic variability [116].

2.2. Black Holes and Their Cosmic Context

The growth of SMBHs is driven primarily by gas accretion and BH-BH mergers. Mergers are expected to dominate low-redshift SMBH growth in dense environments, especially in the high mass range to which the ngEHT will be most sensitive [117–120]. Gas accretion onto SMBHs is a critical piece of the current galaxy formation paradigm, in which feedback from accreting SMBHs is required to regulate gas cooling and star formation in massive galaxies (e.g., [121–123]). At present, however, the details of the feedback processes are poorly understood and are currently the largest source of uncertainty in understanding the combined mass assembly history and evolution of galaxies and their central SMBHs.

The ngEHT will provide unique observational access to both modes of SMBH growth through studies that extend over a vast range of scales (see Figure 8). By beginning to resolve the accretion flows of dozens of AGNs, the ngEHT will enable the extraction of information on their masses, spins, and accretion rates, providing crucial insights into their mass assembly history and growth (Section 2.2.1). In addition, the ngEHT will have sufficient angular resolution to identify sub-parsec binary SMBHs at any redshift, providing a powerful complement to gravitational wave observations of galaxy mergers (Section 2.2.2). In addition, the ngEHT will provide new insights into how SMBHs influence their galactic environments via feedback through multi-wavelength and multi-messenger studies of their relativistic outflows. (Section 2.2.3). We now discuss the goals and requirements associated with each of these objectives.

Figure 8. Conceptual illustration of the science cases explored within the "Black holes and their cosmic context" SWG: BH growth, binary BHs and gravitational waves, and MWL studies of BHs and jets. Credits from left to right: Perimeter Institute, NASA's Goddard Space Flight Center/Jeremy Schnittman and Brian P. Powell, J. C. Algaba for the EHT Collaboration [15]. Composition: Thalia Traianou, IAA-CSIC.

2.2.1. Understanding Black Hole-Galaxy Formation, Growth and Coevolution

The masses and spins of SMBHs encode their assembly history. SMBH masses trace this assembly history in a statistical fashion, with the distribution of SMBH masses—i.e., the BH mass function (BHMF)—capturing the population-level growth and evolution over cosmic time [124]. Measurements of SMBH spin can trace the growth histories of individual objects. For instance, BHs accreting from a thin disk with a steady rotation axis can be spun up to a maximum value of $a = 0.998$ [125], while discrete accretion episodes from disks with random rotation axes will tend to spin a BH down [126]. In addition, BHs accreting at low-Eddington rates for Gyrs can also be spun down due from the energy extraction that is required to power their jets via the Blandford-Znajek process [55,127].

The ngEHT will provide access to SMBH masses by observing the sizes of their horizon-scale emitting regions at (sub)millimeter wavelengths. EHT observations of M87* have demonstrated that measurements of the diameter of the ring-like emission structure can be used to constrain the SMBH mass [6]. The ~11% mass measurement precision achieved using the initial EHT observations of M87*—and even the comparatively modest ~25% precision achieved for the more challenging observations of Sgr A* [12]—establish the

"shadow size technique" as among the most precise means of measuring SMBH masses (see, e.g., [128]). With the additional angular resolution and sensitivity provided by the ngEHT, Pesce et al. [129] estimate that ~50 SMBH masses will be measurable for nearby AGNs distributed throughout the sky (see Figure 9). These measurements will substantially increase the number of SMBHs with precisely-measured masses, improving our understanding of the BHMF in the local Universe.

Relative to mass measurements, observational spin measurements for SMBHs are currently scarce; only roughly three dozen spin measurements are available for nearby SMBHs, with the majority obtained from X-ray diagnostics of the iron K-alpha line [78]. These iron-line measurements are uncertain because the method is highly sensitive to the orbital radius at which the accretion disk's inner edge truncates, which is typically assumed to occur at the innermost stable circular orbit [130]. In addition to their large uncertainties, current X-ray measurements are also biased towards high Eddington ratio objects.
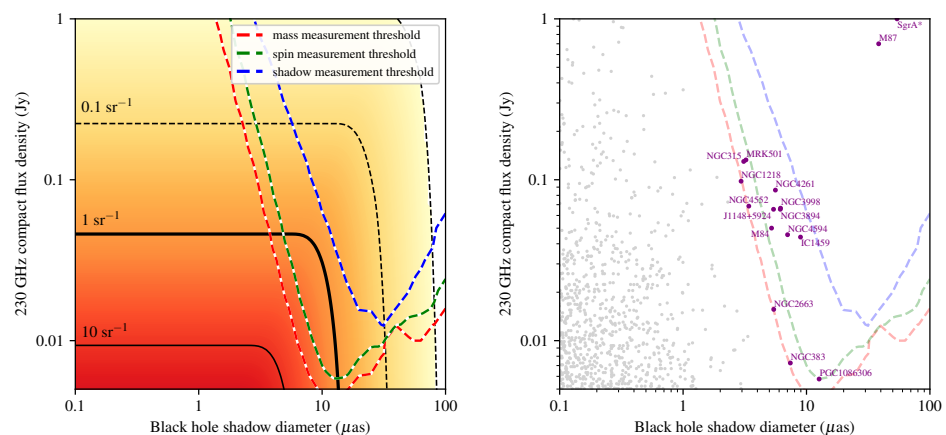
Figure 9. SMBH population studies with the ngEHT. (**left**) Black contours show the estimated cumulative number density of SMBHs as a function of shadow diameter and 230 GHz flux density. Colored contours indicate threshold values at which the ngEHT Phase-1 could plausibly measure the SMBH mass (red), spin (green), and shadow (blue) in a superresolution regime. Reproduced from Pesce et al. [129]. (**right**) Estimated 230 GHz compact flux density and BH shadow diameter for a subset of bright VLBI-detected SMBHs in the ETHER database. Colored lines again indicate the approximate measurement thresholds for the ngEHT Phase-1 array to measure the BH mass, spin, and shadow as shown on the left. Adapted from Ramakrishnan et al. [131].

The ngEHT will provide access to SMBH spins by observing the polarized radio emission emitted by the horizon-scale accretion flows around nearby AGNs. Current EHT observations have provided only modest constraints on the spin of M87* [5,8], but recent and ongoing advances in our theoretical understanding of near-horizon accretion flows will soon enable more precise spin quantifications from similar observations. As detailed in Ricarte et al. [79], linear polarimetric observations made by the ngEHT will provide estimates of SMBH spins by tracing the near-horizon magnetic field structures. The curl of the linear polarization pattern in the emission ring near a SMBH has been shown to correlate with SMBH spin in GRMHD simulations [80,81]. Ongoing studies indicate that this correlation originates from changes in the magnetic field geometry that are associated with frame dragging, which becomes stronger as spin increases [132]. Pesce et al. [129] estimate that the ngEHT will be able to constrain ~30 SMBH spins through measurements of their horizon-scale polarized radio emission. Moreover, the spin measurements enabled by the ngEHT will offer fundamentally new insights by constraining the spins of low Eddington ratio SMBHs—rather than the high Eddington ratio SMBHs preferentially measured using X-ray techniques—which is a regime that is more representative of the overall SMBH population in the Universe.

The estimates from Pesce et al. [133] and Pesce et al. [129] for the number of SMBHs for which the ngEHT can make mass and/or spin measurements are based on statistical considerations, using our current understanding of the local BHMF and the distribution of SMBH accretion rates to predict how many objects should fall within the observable window. However, identifying the specific objects to target with the ngEHT for these measurements requires dedicated observational surveys of AGN to determine which sources are sufficiently bright, massive, and nearby. To this end, the Event Horizon and Environs ([ETHER; [131]]) database aims to provide a standardized catalog of ngEHT targets. Currently, the ETHER sample includes $\sim 10^3$ SMBHs that have been previously observed to have mas-scale structure at cm wavelengths and which have predicted 230 GHz flux densities greater than a few mJy. Of these sources, $\sim$ten have bright 8–86 GHz VLBI detections (from jet emission) and are predicted to be bright enough to image their jet bases at $\lesssim 100\ R_g$ with the ngEHT (see Figure 9). The identification of ngEHT targets with bright accretion inflows but without detected cm-wave jets is ongoing; the currently known ~ 200 BHs with estimated ring sizes $\geq 5\ \mu as$ primarily have (observed arcsec-scale and/or predicted mas-scale) 230 GHz flux densities less than 1 mJy, with the brightest falling in the 1 to 10 mJy range. The upcoming release of the e-ROSITA all-sky hard X-ray survey (with SDSS V and 4MOST spectroscopic followups for BH mass estimates) is expected to significantly expand the list of potential targets in this accretion-inflow-only sample, which will permit definitive specifications on the sensitivity requirement for the ngEHT to measure a large population of horizon-resolved sources.

2.2.2. Understanding How SMBHs Merge through Resolved Observations of Sub-Parsec Binaries

Binary SMBHs are generic products of galaxy mergers, that are thought to drive structure formation in our dark energy-driven cold dark matter Universe. During SMBH mergers, dynamical friction and stellar mass segregation act to draw the two resident massive objects to the center of the merger remnant [134]. The environmental interactions that drive the binary to separations of ~ 0.1–10 pc are understood, but the mechanism(s) that drive continued inspiral beyond this point—and in particular, to the sub-parsec regime in which gravitational wave emission is expected to efficiently complete the merger process—remain unclear (e.g., [135]). A number of solutions to this long-standing and so-called "final parsec problem" [136,137] have been proposed; for instance, interactions with gas in a circumbinary disk, and three-body interactions with stars could all contribute and have significant influence on the shape and evolutionary timescale of the binary. Uncovering the details of the physics in this last parsec informs the science cases of future gravitational-wave detectors such as Pulsar Timing Arrays (PTAs) and space-based gravitational-wave interferometry (e.g., LISA).

The ngEHT will have a nominal angular resolution of 15 μas, which implies a linear resolution of ≤ 0.13 pc across all redshifts. The effective resolving power may be further improved by a factor of several through the use of "super-resolution" techniques (e.g., Chael et al. [138], Akiyama et al. [139], Broderick et al. [140]). The ngEHT can therefore *spatially resolve* SMBH binaries that have entered their steady-state gravitational wave emission phase. The orbital period at this stage is typically short (months to years), which makes it accessible to multi-epoch observations with the ngEHT. Furthermore, D'Orazio and Loeb [141] estimate that between ~ 1 and 30 sub-parsec SMBH binaries should have millimeter flux densities in the $\gtrsim 1$ mJy regime that will be accessible with the ngEHT.

2.2.3. Multi-Wavelength and Multi-Messenger Studies of SMBHs and Their Relativistic Outflows

The EHT has already demonstrated the immense value of extensive multi-wavelength campaigns to augment horizon-scale imaging (e.g., [10,15]), and the ngEHT will similarly benefit from coordinated observations (for a review, see [142]). In particular, the relativistic jets launched by SMBHs extend the gravitational influence of BHs to galactic scales, converting and transporting immense amounts of energy across the full electromagnetic spectrum.

These jets act as powerful particle accelerators that are thought to produce ultra-high energy cosmic rays and have also been implicated in the production of high-energy neutrinos (e.g., [143–148]).

The ngEHT can directly image flaring regions, creating an opportunity to shed light on the physical mechanisms that drive acceleration of protons to PeV energies and generation of high-energy neutrinos. Moreover, crucial insights into the jet composition can be obtained by combining information about the jet dynamics with information about the accretion power (e.g., from X-ray observations). Ideally, this will involve both triggered and monitoring ngEHT observations. Triggered observations would happen when a neutrino arrives within an error region from a strong blazar. Limiting the trigger on both the neutrino energy (above ∼100 GeV) and VLBI flux density (above ∼0.5 Jy) would increase the probability of association and ensure sufficiently high dynamic range of the ngEHT images, respectively. The initial trigger would be followed by ∼monthly monitoring for a year. In addition to this mode, observing a large sample of the strongest blazars with ∼monthly monitoring, supplemented by additional single-dish flux monitoring, will provide an opportunity to study the evolution of sources before neutrino production and to characterize the features that are associated with neutrino production.

In addition, by observing a population of blazars, the ngEHT will be able to measure the jet profile from the immediate vicinity of a SMBH through the acceleration and collimation zones and past the Bondi radius (e.g., [149]). By observing with coordinated multi-wavelength campaigns, the ngEHT will provide decisive insights into the nature of the bright, compact "core" feature that is seen in many blazars (e.g., [150]). Current EHT images of blazars show complex, multi-component emission [16,18,19], so ngEHT observations extending over multiple months to study the evolution of these components will be imperative.

Multi-wavelength and multi-messenger studies of flaring activity in blazar jets will require ngEHT monitoring campaigns with triggering capabilities followed by a cadence of the order of weeks. Full Stokes polarization capabilities with high accuracy (systematic errors on polarization ≲0.1%) and high imaging dynamic range (≳1000:1 to detect faint jet emission) will be required for mapping the magnetic field in the jet regions through Faraday rotation analyses. Close coordination with other next-generation instruments, such as the Cherenkov Telescope Array (CTA), LISA, SKA, ngVLA, and Athena will significantly enrich the potential for multi-wavelength and multi-messenger studies with the ngEHT.

2.3. Accretion

Electromagnetic radiation from SMBHs such as M87* and Sgr A* originates in hot gas, which is brought close to the BH by an accretion disk (for a review of hot accretion flows, see [56]). Some of the same gas is also expelled in relativistic jets or winds. Spatially resolved images of the disk and its associated dynamics provide a remarkable new opportunity to study accretion physics.

BH accretion disks are believed to operate with the help of the magnetorotational instability,[8] which amplifies the magnetic field in the plasma and uses the associated shear stress to transport angular momentum outward [154,155]. Signatures of the magnetic field are revealed via linear and circular polarization of the emitted radiation. Yet, while spatially-resolved and time-resolved spectropolarimetric observations are thus exceptional tools for studying the inner workings of BH accretion, we do not at present have even a single spatially-resolved image of any BH accretion disk.

The closest current results are through EHT observations of M87* and Sgr A*. The ring-shaped 230 GHz emission surrounding a central brightness depression confirms strong light deflection and capture near these BHs. However, the angular resolution and dynamic range achieved so far by the EHT are modest, and it is unclear what part of the observed radiation is from the accretion disk and what is from the jet (see, e.g., [5,13]). The ngEHT will have the sensitivity to image out to larger radii from the BH and to make time-resolved movies in all Stokes parameters. These advances will enable progress on three broad fronts

in accretion physics: revealing the physical mechanism that drives accretion onto SMBHs (Section 2.3.1), observing localized electron heating and dissipation (Section 2.3.2), and measuring signatures of frame dragging near a rotating black hole (Section 2.3.3).

2.3.1. Revealing the Driver of Black Hole Accretion

Our current understanding of accretion close to a BH is largely guided by ideal general relativistic magnetohydrodynamical (GRMHD) numerical simulations (see, e.g., [156,157]). These simulations suggest that the strength and topology of the magnetic field play an important role. When the field is weak and scrambled, the accreting gas becomes turbulent, with eddies over a wide range of length scales (e.g., [158]). When the field is strong, and especially when it also has a dipolar configuration (this is called a "magnetically arrested disk" or MAD; [159]), accretion occurs via large discrete inflowing streams punctuated by episodic outward eruptions of magnetic flux. The ngEHT will be able to identify these and other dynamical patterns in the accretion flow by making real-time movies. Flux-tube eruptions [102,151,152,160], orbiting spiral patterns (e.g., [161]), and bubbling turbulence, could all be accessible to observations. Crucially, spatially-resolved measurements of the linear polarization fraction, degree of circular polarization, and Faraday rotation, will provide rich detail on the magnetic field topology and its strength (e.g., [32]). Different target sources will presumably have different dynamics and field configurations, opening up a fruitful area of research. In the specific case of a MAD system, it is unknown exactly how the strong field originates. One proposal posits that the field is generated in situ by a radiation-driven battery mechanism (e.g., [162]). It predicts a specific relative orientation of the dipolar magnetic field with respect to the accretion disk angular velocity vector. If any of ngEHT's targets is MAD (EHT observations suggest M87* and Sgr A* may both be such systems), testing the predictions of the radiation battery model would be an important secondary goal.

Accretion-related ngEHT science will be primarily enabled through observations of M87* and Sgr A*, with two major associated challenges. First, the most interesting effects occur in regions of the disk within a few event horizon radii. However, this is precisely where the observed image is highly distorted by the gravitational lensing action of the BH, the same effect which produces the ring image of M87*. Disentangling lensing to reveal the true underlying structure of the accretion disk will require new image processing techniques. Second, the observed image will often be a superposition of radiation from the accretion disk and the jet. The two components will need to be separated. One promising method is to utilize dynamics and variability, which can be quite different in the disk and in the jet. Observations with a cadence of t_g would be ideal to study the most rapid variability, and interesting variations are expected on all timescales up to 10^3–10^4 t_g. Full-night observations with sufficient baseline coverage for snapshot imaging on sub-minute timescales will needed for Sgr A*, while a monitoring campaign with a sub-week cadence and extending for at least 3 months (and, ideally, over multiple years) will be ideal for M87*.

2.3.2. Localized Heating and Acceleration of Relativistic Electrons

The radiation emitted from an accretion disk is produced by hot electrons, which receive their heat energy via poorly-understood plasma processes in the magnetized gas. The most promising idea for heating is magnetic reconnection, which can occur in regions with large-scale topological reversals of the magnetic field, or in regions with large shear, or where small-scale turbulent eddies dissipate their energy. All of these processes are at their most extreme in the relativistic environment found in BH accretion disks.

Our current understanding of relativistic magnetic reconnection is based on particle-in-cell (PIC) simulations (e.g., [163–166]). These numerical studies show clear evidence for unequal heating of electrons and ions, as well as acceleration of both into a non-thermal distribution with a power-law tail at high energies. Electron heating in large flares in BH disks would be especially interesting for ngEHT observations. A flare may initially appear as a bright localized region in the image. It will subsequently move around the image, will

also likely spread to become more diffuse, and will show effects from graviational lensing (see, e.g., [95,97,102,167]). Both the ordered motion of the heated region and its spreading will provide fundamental information on the microscopic plasma physics processes. The heated electrons will also cool as they radiate, causing the electron distribution function (eDF) to evolve. Multi-wavelength imaging will provide a handle on both the dynamics and the eDF evolution.

Less dramatic steady heating should also be present, and it will likely show strong variations as a function of radius in both amplitude and eDF. With the enhanced dynamic range of the ngEHT, these spatial variations should be accessible over a factor of 10 range of radius. Particle acceleration and heating is relevant for a wide range of astrophysical phenomena. While we have some information on low energy processes from laboratory experiments and measurements in the solar wind, there is currently no observational technique for direct study of heating in relativistic settings. Imaging BH accretion disks with the ngEHT can reveal localized heating and acceleration on astrophysical scales and will track the evolution of the energized electrons. Lessons from such observations would have a widespread impact in many other areas of astrophysics.

2.3.3. Dynamical Signatures of Frame Dragging Near a Rotating Black Hole

Direct observations of the inner region of the accretion disk provide an opportunity to study the object at the center, namely, the BH itself. While the most significant effect on large scales is the immense gravitational pull of a BH, another gravitational property of these objects is arguably even more interesting. Namely, a spinning BH has the remarkable property that it drags space around it in the direction of its spin. This so-called frame-dragging effect is felt by all objects outside the BH, including the accretion disk. The effect is strongest in regions within a few event horizon radii of the BH.

Spatially-resolved and time-resolved imaging has the potential to confirm the frame-dragging effect and to study its details (see, e.g., [168]). Since the accretion disk is fed by gas at a large distance from the BH, the outer disk's angular momentum vector is likely to be randomly oriented with respect to the BH spin axis. Only when gas comes close to the BH does it feel the spin direction of the BH via frame-dragging. The manner in which the disk adjusts its orientation can provide direct confirmation of the frame-dragging phenomenon. If the disk is tilted with respect to the BH spin vector, it is expected to precess and align with the BH inside a certain radius (see, e.g., [5]). Both the precession and alignment can be observed and studied by the ngEHT. In the special case of a retrograde accretion flow (i.e., when the disk's orbital motion is in the opposite direction to the BH spin), the angular velocity of the disk gas will reverse direction close to the horizon. There will be a related effect also in the orientation of the projected magnetic field, which may be visible in polarimetric ngEHT images. Observing these effects directly with the ngEHT would be a breakthrough achievement and would provide a new tool to study a central prediction of the Kerr spacetime (see also Section 2.1.2).

2.4. Jet Launching

Relativistic jets are among the most energetic phenomena in our universe, emitting radiation throughout the entire electromagnetic spectrum from radio wavelengths to the gamma-ray regime, and even accelerating particles to highest measured energies (for a review, see [169]). The most powerful jets are those that are anchored by nuclear SMBHs in AGN, as emphatically demonstrated through the images of M87* with the EHT. Yet, despite this impressive breakthrough, the actual jet launching mechanism and power source is still uncertain. The ngEHT has the potential to make pivotal discoveries related to the power source of relativistic jets (Section 2.4.1), and to the physical conditions that launch, collimate, and accelerate these jets (Section 2.4.2).

2.4.1. Jet Power and Black Hole Energy Extraction

According to our current theories, jets can either be powered by the liberation of gravitational potential energy in the accreting material (e.g., [170]) or by directly extracting the rotational energy of a spinning BH [55]. In both processes, magnetic fields must play a crucial role. Therefore, measuring the velocity field of the innermost jet regions and comparing de-projected rotation of the magnetic fields with the rotation of the BH ergosphere will probe whether jets are launched by rotating BHs.

The ideal target to address this question is M87* because of its large BH mass ($M \approx 6.5 \times 10^9 \, M_\odot$), proximity ($D \approx 16.8 \, \mathrm{Mpc}$), and prominent jet ($P_{\mathrm{jet}} \gg 10^{42} \, \mathrm{erg/s}$). Sgr A* also provides an important target to study—despite decades of VLBI observations, there is no firm evidence for a jet in Sgr A* at any wavelength. Nevertheless, there are compelling reasons to continue the search for a jet in Sgr A* with the ngEHT, including the potential for interstellar scattering to obscure the jet at longer wavelengths (e.g., [171]), evidence for an outflow in frequency-dependent time lags during flares (e.g., [172,173]), and the fact that favored GRMHD models for Sgr A* based on constraints from EHT observations predict the presence of an efficient jet outflow [13]. Comparing the jets in M87* and Sgr A*, together with knowledge of their respective BH properties, will provide fundamental insights into the role of the BH and its environment in producing a jet.

Current EHT observations are limited both in terms of the baseline coverage and image dynamic range, which prohibits estimates of physical parameters in the critical region just downstream of the BH. The ngEHT will provide superior baseline coverage and increased dynamic range, allowing reconstructed movies that simultaneously resolve horizon scale structure and the jet base in M87* and Sgr A*. To identify the source of the jet's power with the ngEHT will require estimates of the magnetic flux threading the SMBH, the spin of the SMBH (see Section 2.1.2), and the total jet power. These estimates will require high-fidelity polarized and multi-frequency images with an angular resolution of ∼15 µas (a spatial resolution of $\approx 4GM/c^2$) and with sufficient dynamic range to simultaneously study both the near-horizon magnetosphere and the jet over many dynamical timescales.

2.4.2. Physical Conditions and Launching Mechanisms for Relativistic Jets

The ngEHT has the potential to substantially improve our understanding of the mechanisms that launch, collimate, and accelerate relativistic jets by measuring the physical conditions at the jet base. For instance, multi-frequency VLBI observations at cm-wavelength mainly probe the extended jet regions and have revealed that the energy distributions of relativistic electrons responsible for the emission follow power-laws. This is in marked contrast to the recent EHT observations of the horizon scale structure around M87* and Sgr A*, which has been successfully modeled using thermal distributions of electrons [5,13]. Important questions therefore arise regarding which physical mechanisms are able to accelerate the thermal particles, and where this particle energization occurs. Using multi-frequency observations at 86 GHz and 230 GHz while making use of VLBI synergies with the next-generation Very Large Array (ngVLA), the spectral index distribution of the radio emission can be mapped at high resolution, allowing estimates of the underlying eDF and indicating possible particle acceleration sites. In addition, linear polarization studies will reveal the magnetic field structure and strength in the jet, and circular polarization will reveal the plasma composition (leptonic/hadronic), opening a window to more detailed understanding of jet microphysics (e.g., [174]).

According to recent GRMHD models, a dynamic range of ∼10^4 will enable us to probe the jet in M87* at a wavelength of 1.3 mm on scales of hundreds of microarcseconds and to reliably measure the velocity profile. In addition to the aforementioned array requirements, monitoring of the jet with cadences of days to weeks is required (for M87*, 1 day corresponds to roughly $3t_g$). Figure 10 shows simulated ngEHT reconstructions of the M87* jet, illustrating the ability of the ngEHT to conclusively identify and track kinematic structure throughout the jet. Finally, in addition to M87*, there are several other potential AGN targets (e.g., Cen A, 3C120, 3C84) of comparable BH mass and distance, which can

also serve as laboratories to study jet launching activity. More distant AGN ($z > 0.1$) would require imaging on a ∼monthly basis.
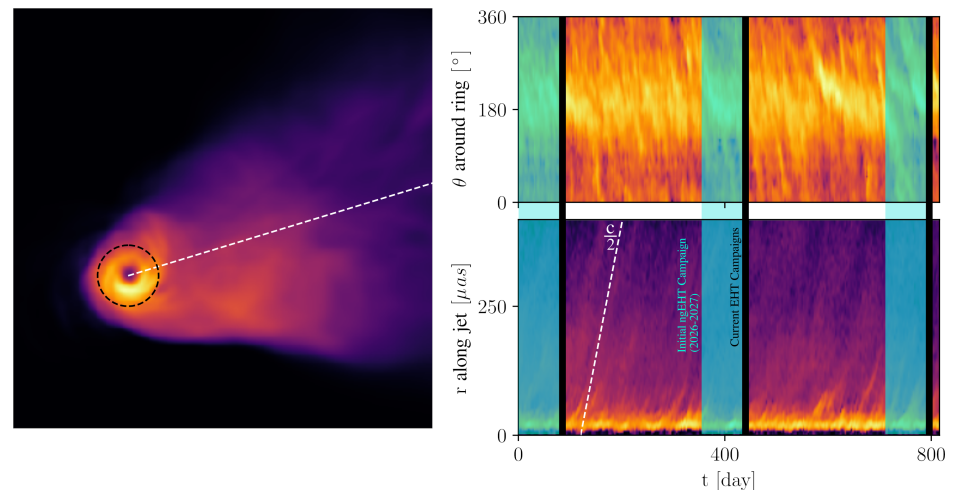
Figure 10. Studying accretion and jet dynamics with the ngEHT. (**left**) A frame from a simulated movie of M87* [175]. (**right**) Azimuthal (**top**) and radial (**bottom**) brightness variations in a reconstructed movie of M87* using ngEHT Phase-1 coverage. The top panel shows how azimuthal variations around the black dashed circle track orbital dynamics near the BH, evident here as diagonal striations with sub-Keplerian angular velocity. The bottom panel shows how radial variations along the white dashed line will reveal the SMBH-jet connection and measure acceleration within the jet-launching region. Initial ngEHT monitoring campaigns (light blue vertical bands) will span 3 months per year with a dense (sub-week) observing cadence; for comparison, current EHT campaigns (dark vertical bands) only span ∼2 weeks per year, which is insufficient to measure the dynamics of the accretion disk or jet.

2.5. Transients

Astrophysical transients are the sites of some of the most extreme physics in the present-day universe, including accreting sources such as BH X-ray binaries and Tidal Disruption Events, explosive events such as supernova as well as the LIGO/VIRGO gravitational wave bursts associated with neutron star-neutron star mergers such as GW170817 [176,177].

In essentially all cases, the radio emission from these transients corresponds to synchrotron emission from relativistic electrons spiralling in magnetic fields either in a jet or in structures which have been energised by a jet associated with the transient (e.g., [178–182]). As with supermassive BHs in AGN, probing the formation, propagation and ultimate energetics of these jets is central to understanding the physics of BHs and how they convert gravitational potential energy of infalling matter into powerful collimated outflows.

Because the field of astrophysical transients is so diverse, we have chosen to focus the ngEHT key science goals and associated requirement related to transients on two sets of objects: BH X-ray binaries (Section 2.5.1) and extragalactic transients (Section 2.5.2). Together, these categories span most of the range both in the astrophysics under study and in the technical requirements for the ngEHT.

2.5.1. Dynamics of Black Hole X-ray Binaries

Black hole X-ray binaries (BHXRBs) represent the bright end of the population of massive stellar remnants in our galaxy. They are expected to number in the few thousands among a likely population of ∼10^8 stellar mass BHs in our galaxy, with a typical mass around $7M_\odot$. They accrete, usually intermittently, from a close binary companion and often reach accretion rates close to the Eddington limit. In other words, they are around

five (eight) orders of magnitude less massive than Sgr A* (M87*) and are accreting at $> 10^7$ times higher Eddington-ratioed rates. There are good reasons, and indeed much circumstantial evidence, to suggest that the coupling between accretion 'states' and jet formation at high Eddington ratios are similar between supermassive and stellar-mass BHs, so their study genuinely, and dramatically, extends the parameter space of study of BHs (e.g., [183,184]).

The event horizons of these stellar-mass BHs will likely never be resolvable by conventional telescopes, but remarkably it has been established that high-time resolution X-ray variability studies of BHXRBs probe the same range of scales in gravitational radii, $r_g \equiv GM/c^2$, as the direct EHT imaging of M87* and Sgr A*. Furthermore, decades of work has established good, but not yet precise enough, connections between characteristic patterns of variability, arising from within $100r_g$, and the formation and launch of the most powerful jets.

With the ngEHT, we will be able to probe BHXRB jets on scales around $10^6 r_g$, at which scales bright (sub-)mm flares often have flux densities in excess of 1 Jy and evolve considerably on timescales of *minutes* (e.g., [185–187]). VLBI studies of jets at ten times larger angular scales have provided the most precise determination of jet launch time (and the corresponding activity in the accretion flow), evidence for strong directional variation and precession of the jet, and circumstantial evidence for interactions and—presumably—internal shocks between components moving at different speeds. This is also the region in r_g in which the jets of M87* and other AGN have been seen to switch from an initially parabolic to a later conical cross section (e.g., [149,188–191]). With the ngEHT, we can directly test if this same collimation is occurring in BHXRB jets. Finally, we now know from the ThunderKAT project on MeerKAT [192] that large-scale jets from BHXRBs which decelerate and terminate in the ISM on timescales of ∼1 year are common (rate of 2–4/year): therefore only in this class of object can we track events from their creation and launch in the accretion flow through to their termination, providing an opportunity for precise calorimetry of their kinetic power.

2.5.2. Extragalactic Transients

The broad term of extragalactic transients encompasses sources including Gamma Ray Bursts (GRBs), Tidal Disruption Events (TDEs), neutron star mergers, supernovae, fast radio bursts (FRBs), fast blue optical transients (FBOTs) and other related phenomena. The origin of the radio emission from these objects is often within relativistic jets, but it may also be more (quasi-)spherical.

Some of these phenomena remain optically thick and bright at (sub-)mm wavelengths for a considerable period of time (months; e.g., [193,194]) which places far less stringent requirements for response and scheduling of ngEHT. Nevertheless, there is a wide range of important physics which could conceivably be tackled, such as whether or not jets are being produced commonly (very topical for TDE jets, which may even be associated with neutrino production) and how much kinetic power was released in the event. Thus, the ngEHT could make significant discoveries by measuring the kinetic power, physical structure, and velocity in extragalactic transients such as GRBs, GW events, TDEs (e.g., [195]), FRBs, and FBOTs.

2.6. New Horizons

The "New Horizons" SWG was formed to explore and assess non-traditional avenues for ngEHT scientific breakthroughs. This group has examined topics including terrestrial applications such as planetary radar science, geodesy, and improved celestial reference frames [196,197]; studies of coherent sources including magnetars, masers, and fast radio bursts; and precise astrometry of AGN [198]. We now describe the two key science goals that have been identified by this SWG, both with cosmological applications: measurements of proper motion and parallax for a sample of AGN at distances up to ∼80 Mpc (Section 2.6.1), and studies of SMBHs and their accretion disks using water vapor megamasers, which

can provide accurate measurements of the Hubble constant up to distances of $\sim$50 Mpc (Section 2.6.2).

2.6.1. Proper Motions and Secular (CMB) Parallaxes of AGN

The multi-band capabilities of the ngEHT will enable the use of the source-frequency phase referencing ([SFPR; [199]]) technique, potentially achieving $\sim$µas-level astrometry for targets that are sufficiently bright and close to known reference sources [46,47]. In addition to many other scientific applications such as measurements of (chromatic) AGN jet core shifts (e.g., [200–202]) and the (achromatic) orbital motions of binary SMBH systems (e.g., [141]), one of the opportunities afforded by this astrometric precision is a measurement of the so-called "cosmological proper motion" [203] or "secular extragalactic parallax" [204]. Because the Solar System is moving with respect to the cosmic microwave background (CMB) with a speed of $\sim$370 km s^{-1} [205], extragalactic objects in the local Universe should exhibit a contribution, $\mu_{\rm sec}$, to their proper motion from the Solar Systems's peculiar motion:

$$\mu_{\rm sec} \approx \left(0.018\,\mu\text{as year}^{-1}\right) \left(\frac{H_0}{70\,\text{km s Mpc}^{-1}}\right) \frac{|\sin(\beta)|}{z}, \tag{1}$$

where z is the object's cosmological redshift, H_0 is the Hubble constant, and β is the angle between the location of the source and the direction of the Solar System's motion with respect to the CMB [203]. An object located at a distance of 10 Mpc ($z \approx 0.0023$) is thus expected to have $\mu_{\rm sec} \sim 8\,\mu\text{as year}^{-1}$, while an object located at a distance of 100 Mpc ($z \approx 0.023$) is expected to have a proper motion of $\mu_{\rm sec} \sim 0.8\,\mu\text{as year}^{-1}$. By measuring the proper motion of many objects and using multi-frequency observations to mitigate chromatic effects in time-variable core shift effects (see, e.g., [206]), the ngEHT could thus isolate the contribution of $\mu_{\rm sec}$ and provide coarse estimates of H_0 that are independent of standard methods (e.g., [207–210]).

2.6.2. Studies of Black Hole Masses and Distances with Megamasers

Water vapor megamasers residing in the molecular disks around nearby AGNs on scales of $\sim$0.1 pc ($\sim$10$^5\,r_{\rm g}$) have proven to be powerful tools for making precise measurements of SMBH masses (e.g., [211,212]), geometric distances to their host galaxies (e.g., [213,214]), and the Hubble constant (e.g., [209,215]). While the majority of the research carried out to date has utilized the 22 GHz rotational transition of the water molecule, other transitions are expected to exhibit maser activity under similar physical conditions as those that support 22 GHz masers [216,217]. In particular, both the 183 GHz [218,219] and the 321 GHz [220–223] transitions have been observed as masers towards AGN. The latter transition falls in the ngEHT observing band, as does another tranisition at 325 GHz that is also expected to exhibit maser activity [224].

Observations of water megamaser systems with the ngEHT will necessarily target transitions such as those at 321 GHz and 325 GHz, rather than the transition at 22 GHz. If the submillimeter systems are as bright as those at 22 GHz, then the >order-of-magnitude improvement in angular resolution brought about by the ngEHT will impart a corresponding improvement in the precision of maser position measurements in these systems. However, the typical brightness of submillimeter megamaser systems is currently unknown, and the two sources that have to date been observed at 321 GHz both exhibit fainter emission at 321 GHz than at 22 GHz [220,221]; it is thus possible that systematically fainter submillimeter transitions (relative to 22 GHz) will offset the improvement in position measurement precision through reduced signal-to-noise ratios. Nevertheless, even comparable measurement precisions for submillimeter transitions will provide a statistical improvement in the mass and distance constraints for systems observed in multiple transitions. Furthermore, because the optimal physical conditions (e.g., gas temperature and density) for pumping maser activity differ between the different transitions, simultaneous measurements of multiple transitions in a single source may be used to provide constraints on those physical conditions [216,217]. It is also possible that future surveys will uncover populations of AGN

that exhibit submillimeter maser activity but no 22 GHz emission, thereby increasing the sample of sources for which the megamaser-based measurement techniques can be applied.

2.7. Algorithms and Inference

The results produced by the EHT collaboration have been enabled by a suite of new calibration, imaging, and analysis softwares, many of which were custom-built to tackle the unique challenges associated with the sparsity and instrumental corruptions present in EHT data as well as with the rapid source evolution and scattering in Sgr A* (e.g., [138–140,225–239]). Many of the difficulties that motivated imaging developments for the EHT are expected to be compounded in ngEHT observations, with a large increase in data volume (increased bandwidth, more stations, and faster observing cadence), dimensionality (multi-frequency and multi-epoch), and requisite imaging fidelity (larger reconstructible field of view and higher imaging dynamic range). The next generation of algorithmic development is already underway, with new data processing [240,241], imaging [31,75,242], machine learning [81], and full spacetime [81,82,97,234,243] methods being designed to address the challenges and opportunities associated with ngEHT data.

To assess the scientific potential of the ngEHT, inform array design, and prompt the development of new algorithms, the ngEHT has launched a series of Analysis Challenges [34]. For each challenge, synthetic (ng)EHT datasets are generated from theoretical source models. These datasets are made available through the ngEHT Analysis Challenge website[9] and are accessible to anyone upon request. Participants then analyze the data by, e.g., reconstructing an image or fitting a model, and submit their results through the website. All submissions are evaluated with metrics quantifying, e.g., data fit quality or similarity of image reconstructions to the ground truth source model.

Challenge 1 focused on static source models of Sgr A* and M87* at 230 and 345 GHz, and was set up mainly to test the challenge process and infrastructure. Challenge 2 was more science oriented, and focused on movie reconstructions from realistic synthetic observations of Sgr A* and M87* at 86, 230, and 345 GHz. Both challenges received submissions from a broad array of reconstruction methods. Figure 11 shows two submitted movie reconstructions from Challenge 2. The M87* reconstruction shows the ngEHT's ability to reconstruct both the BH shadow and extended jet dynamics at high dynamic range, allowing detailed studies of jet launching. The Sgr A* shearing hotspot reconstruction, based on [97] and motivated by the observational results of GRAVITY Collaboration et al. [244], shows the ngEHT's ability to reconstruct rapid (intra-hour) accretion dynamics, even in moderate weather conditions at 230 GHz. In general, Roelofs et al. [34] found that standalone 345 GHz imaging of the M87* jet or Sgr A* dynamics is challenging due to severe atmospheric turbulence and optical depth effects. However, multi-frequency reconstructions showed that by utilizing information from 86 and 230 GHz, the M87* jet may be reconstructed at 345 GHz (see also [31]). Additionally, while the Sgr A* shearing hotspot orbit could be reconstructed well, variability in GRMHD simulations was found to be more challenging to reconstruct due to the more turbulent nature of the plasma.

Two additional challenges are being run. Challenge 3 focuses on polarimetric movie reconstructions, and Challenge 4 will focus on science extraction, particularly to attempt measurements of the BH photon ring and the spacetime parameters. The merit of frequency phase transfer techniques for multi-frequency imaging will also be investigated (see also [45]).

2.8. History, Philosophy, and Culture

The History, Philosophy, and Culture (HPC) SWG includes scholars from the humanities, social sciences, and sciences. HPC Key Science Goals were developed across four focus groups: Responsible Siting (Section 2.8.1), Algorithms, Inference, and Visualization (Section 2.8.2), Foundations (Section 2.8.3), and Collaborations (Section 2.8.4). We will now briefly summarize a selection of these goals that have been prioritized; for a more complete description, see HPC White Paper [52].
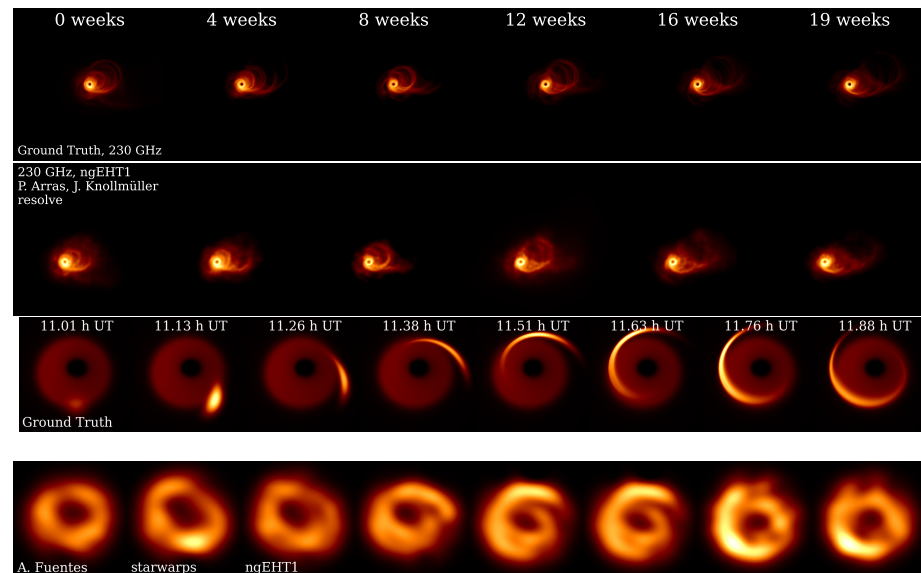
Figure 11. Example ngEHT reconstructions for Sgr A* (top two rows) and M87* (bottom two rows), using submissions for the second ngEHT Analysis Challenge [34]. For each source, upper panels show ground truth movie frames, and lower panels show example reconstructions. The M87* ground truth movie is a GRMHD simulation generated with H-AMR [245] and ray-traced with `ipole` [246]; the reconstructed movie was produced using `resolve` [225]. The Sgr A* simulation is a semi-analytic accretion flow with a shearing hot spot [97,247]; the reconstructed movie was produced using `StarWarps` [248]. Panels are reproduced from Roelofs et al. [34].

2.8.1. Responsible Siting

Telescope siting has, historically, relied almost entirely upon ensuring that sites meet technical specifications required for observation including weather, atmospheric clarity, accessibility, and cost. As the issues at Mauna kea in Hawai'i show,[10] telescopes exist within a broader context and, as they choose sites, scientific collaborations incur the obligation to address ethical, social, and environmental specifications alongside technical ones.

The ngEHT has already hosted a workshop dedicated to advancing responsible siting practices, which drew together experts in a wide range of fields including philosophy, history, sociology, advocacy, science, and engineering.[11] This workshop was run by a dedicated siting focus group within the ngEHT HPC SWG, aimed at addressing the broader impacts of constructing and operating the chosen sites, with the goal of guiding short- and long-term siting decisions. Of particular interest to the group is consultation with areas outside of astronomy which also face questions of responsible siting including biotechnology[12], archaeology and paleontology[13], physics[14], and nuclear technologies[15]. Ultimately, the goal is to model the decision-making process by joining technical, environmental, and community concerns, and to arrive at explicit guidelines that could assist with future siting challenges.

For the ngEHT to achieve its goals on responsible siting, a number of concrete steps are necessary. First, the collaboration must integrate social and environmental impacts into its siting decisions, initially, via the inclusion of ethicists, social scientists, environmental experts, and local community advocates in siting meetings who will contribute to the decision-making process as well as the inclusion of explicit cultural, social and environmental factors in siting decision metrics; later, via the creation and performance of explicit community impact studies, in addition to reviewing the environmental impact studies already performed as part of the standard siting. These studies will embrace surveys of local social factors for sites to aid in the decision process and will involve on-site community consultation as well as work with local government and academic structures.

Second, the collaboration must ensure that when telescopes are built, the building process is collaborative and non-extractive as well as sensitive to the history and culture of local communities and the lands in consideration. This goal will require establishing an ongoing dialogue with local community groups as early as possible in the siting process, and setting up explicit agreements that are mutually beneficial to all parties. As such, funding for community consultation and projects is a central part of the funding structure for the ngEHT; the aim is to ensure that local educational, scientific, and economic opportunities are built into the project from the out-set. This will involve examining local relationships with existing sites to be supplemented with new technology, as well as forging new relationships where un-developed sites are under consideration. The ngEHT project will be carefully considering who is at the table, and ensuring all local groups that may be impacted have a voice in the process. The ngEHT will also aim to work to integrate local and traditional knowledge into this process, recognizing that these are not in tension with scientific knowledge, but are continuous with it. Moreover, each site will be unique, with different needs and histories that will inform the kinds of relationships that will develop. As such, part of the community impact study will need to detail what sort of benefits local communities may want from, as well as offer to, the ngEHT collaboration. Possibilities include improved infrastructure, education funding, outreach, and knowledge exchange under terms and conditions that meet the needs of the communities in question.

The ngEHT must also accept the fact that community, environmental, and cultural aspects may prevent a site from being developed, and that a 'no' from locals is a legitimate outcome. A clear goal, then, is to work with community siting experts from both inside and outside astronomy to establish what a 'no' looks like, as well as a 'yes', and to develop norms and practices which can help survey local groups to ensure their voices are being heard.

Third, the ngEHT aims to minimize its environmental impact, including careful consideration of how construction and development of sites may impact native ecosystems as well as actively planning for what the eventual decommissioning and subsequent environmental repair of a site will look like. The ngEHT is committed, wherever possible, to using environmentally friendly techniques, technology, and materials, including in energy-efficient data-storage and computing.

Finally, a major goal of this focus group will be the production of one or more papers detailing current best-practices for responsible telescope siting. Here, the initial three to five sites (i.e., those in the ngEHT Phase-1) will be treated as proof-of-concept sites where norms can be designed and established, and experts from both inside and outside astronomy will be brought in to help guide the paper writing process.

2.8.2. Algorithms, Inference, and Visualization

The ngEHT is a long-term project which will heavily rely on software supported modes of reasoning, including imaging algorithms for image reconstruction, and GRMHD simulations and relativistic ray tracing codes for parameter extraction. Philosophers of other sciences relying on computer simulations (including climate sciences and theoretical cosmology) diagnosed that problematic features might arise in such situations. These include [266,267] (i) kludging: temporary and ad hoc choices (concerning, e.g., values of parameters, or a manner of merging together two pre-existing fragments of code) made for convenience and without principled justification; (ii) generative entrenchment: contingent choices made during code development in order to deal with problems arising in particular contexts are baked in and transferred to future versions; over time, awareness of the origin of various fragments might be lost; (iii) confirmation holism: assigning success or failure of a numerical model as a whole to a particular fragment of code becomes very hard. Some of these problematic features may have positive elements—for example, feature (i) makes code development faster than if it were properly documented; feature (ii) might represent consensus of the collaboration. Awareness of these features and development of active means of preventing their negative effects will make inference methods of the ngEHT more reliable.

Further, new inferential methods based on various forms of machine learning and artificial intelligence are becoming increasingly widespread, including in astronomy. Such methods come with many benefits, including much faster data processing times, but also with drawbacks, including a lack of epistemic transparency (the inner workings of a machine learning model are not easily available or even understood by its users, in contrast with the steps taken by a more traditional imaging or parameter extraction algorithm), and risk of building in bias through training on data sets containing untested assumption about the target system. Frameworks for mitigating these risks, so-called explainable artificial intelligence, have been developed (e.g., [268–270]). We will systematically evaluate these methods and motivations behind them, isolating those which can and which should be applied to future ngEHT data analysis pipelines.

Reception of astronomical images takes place in a broader context of visual culture, and we will consider the importance of aesthetic choices made during production, such as assignment of color to underlying physical parameters or landscape associations invoked by the resulting image (e.g., Kessler [271]; HPC White Paper [52]). As for the EHT, images produced by the ngEHT will shape public perception of black holes and astronomy. Analysis of such cultural factors will help with being intentional about the impact and perception of images—inside and outside the technical community. Accordingly, procedures for systematically including such choices and for testing whether an image succeeds in conveying the intended connotations will be developed, and applied, for example, to future polarization data and multi-frequency images.

The requirement to achieve long-term reliability of ngEHT inferences will necessitate the identification of inference methods deemed undesirable, and development of software evaluation tests to ameliorate those features. Improving image presentation will focus attention on cultural factors that shape audience reactions to visualizations—in turn, we will need to develop comprehension tests probing audience responses.

2.8.3. Foundations

The Foundations focus group complements the Fundamental Physics working group, providing a different, critical lens for thinking about what the ngEHT observations can tell us about fundamental physics. The ngEHT results will both be informed by, and inform, philosophical and historical perspectives on issues such as scientific representation and modeling, idealization, underdetermination, theory testing (confirmation), and more (Section 3, [52]). This focus group facilitates ongoing interdisciplinary discussions of foundational issues, in parallel with discussions in fundamental physics.

2.8.4. Collaborations

A fully integrated working group of scholars from the social sciences and humanities within a STEM collaboration provides an unprecedented opportunity to optimize the collaboration structure from the very beginning. Our main goal is a structure that enables, encourages, and emphasizes transparent decision-making, diversity, fair credit assignment and accountability (Section 4, [52]).[16] This translates directly into various requirements for the ngEHT collaboration, as detailed further below.

In addition, a long-term Forecasting Tournament [287,288] will clarify the ngEHT decision-making process. Participants' judgments about the outcome of ngEHT experiments and observations will reveal the novelty of eventual results and will elucidate the process of hypothesis generation and testing. By systematically collecting predictions, we will be able to track the return on testing different hypotheses, identify unresolved ambiguities within the design or implementation of an experiment (which may lead to new areas of investigation) and develop a more (cost) effective research management strategy [289]. There are also direct epistemic advantages to surveying predictions and expectations. The EHT already went to great lengths to counteract a quite natural tendency to halt image reconstruction when the images coincided with anticipated results (for example, blind trials with known, simulated data; autonomous imaging groups who did

not share intermediate results; [4]). In the ngEHT, imaging programs will become more elaborate, use of AI more extensive, and data volumes will expand rapidly. Therefore it will be increasingly important for the collaboration to be aware of forecasted results—precisely to avoid premature confirmation.

These goals require frequent monitoring and evaluation of the internal communication structure and climate. This will be achieved via the complementary methods of surveys, interviews, and network analysis tools from the digital humanities (HPC White Paper [52]).[17] This will require that at least some collaboration members be available for interviews and surveys. Only against the backdrop of this ongoing feedback loop will it be possible to ensure the long-term effectiveness of the following further requirements: (a) a governance structure that includes a central, representative, elected body, as well as a standing ethics committee responsible for the creation, adherence to, and updating of the collaboration's Community Principles and Code of Conduct—see HPC White Paper [52] for a tentative proposal; (b) an authorship and membership model tailored to the needs of a modern collaboration involving members from a diverse group of (scientific and non-scientific) cultures, i.e., a model that accounts for fair distribution of credit and accountability and allows for and realizes the value of dissenting opinions.[18] A dedicated task force has begun developing such a model.

3. Summary

The ngEHT project has undergone a multi-year design process to define community-driven science priorities for the array. This process has identified breakthrough science related to studies of BH spacetimes, as well as a wealth of new opportunities beyond what has been explored with past EHT experiments. These science opportunities arise from the potential to substantially expand upon the currently explored parameter space:

- Improved angular resolution and image fidelity through increased sensitivity and baseline coverage. These enhancements are the most significant requirements for studies of fundamental physics with the ngEHT.
- Expanding from independent multi-band observations to simultaneous multi-band observations at 86, 230, and 345 GHz. This upgrade will substantially improve the EHT's sensitivity to observe faint sources, dim extended emission, and compact structure on the longest baselines at 345 GHz, especially through the use of multi-frequency phase transfer.
- Adding more sites to enable "snapshot" imaging of variable sources including Sgr A*, and extending observing campaigns over multiple years. Together, these upgrades will improve the temporal sensitivity of current EHT observations by ∼5 orders of magnitude, enabling a wealth of new variability studies (see Figure 2).

We have classified each of the key science goals discussed in Section 2 as either *Threshold* or *Objective*. Threshold science goals define the minimum target that the array concept is designed to meet. Objective science goals are additional major science opportunities or stretch target for the array concept to meet. This classification does not indicate the relative merit of the science objective; some goals are assigned as objective because they are considered to be too speculative or high-risk (e.g., studies of the photon ring and frame dragging), insufficiently unique to the ngEHT (e.g., studies of axions and SMBH binaries), or too poorly understood to define a precise associated instrument requirement that will guarantee success (e.g., studies of extragalactic transients). Table 1 provides the categorization of each goal. In addition, we have developed a set of homogeneous array requirements for the science goals in the framework of a Science Traceability Matrix (STM). A representative subset of the STM is given in Figure 12.

Table 1. Key Science Goals of the ngEHT.

Threshold Science Goals
• Establish the existence and properties of black hole horizons
• Measure the spin of a SMBH
• Reveal black hole-galaxy formation, growth and coevolution
• Reveal how BHs accrete material using resolved movies on event horizon scales
• Observe localized heating and acceleration of relativistic electrons on astrophysical scales
• Determine whether jets are powered by energy extraction from rotating BHs
• Determine the physical conditions and launching mechanisms for relativistic jets

Objective Science Goals
• Constrain the properties of a BH's photon ring
• Constrain ultralight boson fields
• Determine how SMBHs merge through observations of sub-parsec binaries
• Connect SMBHs to high-energy and neutrino events within their jets
• Detect frame dragging within the ergosphere of a rotating BH
• Measure the inner jet structure and dynamics in BH X-ray binaries
• Detect the kinetic power, physical structure, and velocity in extragalactic transients
• Detect proper motions and secular (CMB) parallaxes of AGN up to ∼80 Mpc distances
• Leverage AGN accretion disk megamasers to measure their AGN host properties

Key Science Goal († = threshold science goal)	M87*	Sgr A*	Other SMBH	Transient	Other	Physical Parameter	Observable	Mode	Cadence	Frequency (GHz)	Freq. Phase Transfer	ngEHT Phase
Fundamental Physics												
†Establish the existence and properties of black hole horizons	X	X				Lensed image of the horizon	Measure brightness and shape of the dimmest region of the apparent shadow	Single Observation	Single campaign with full array	230+345	Yes	M87*: 1 Sgr A*: 2
†Measure the spin of a SMBH	X	X				SMBH dimensionless spin	Average polarization spiral (β-phase) over 10 epochs at 230 and 345 GHz	Multiple Observations	M87*: 10 observations separated by >1 month; Sgr A*: 10 full nights with full array	230+345	Yes	
Constrain the properties of a black hole's photon ring	X	X				n=1 photon ring	Statistically significant detection of persistent thin ring feature	Multiple Observations	M87*: 3 observations separated by >1 month; Sgr A*: 3 full nights with full array	230+345	Yes	M87*: 1 Sgr A*: 2
Constrain ultralight boson fields	X	X				Superradiance from clouds of sub-eV ultralight bosons	Polarization angle oscillation along the photon ring and spin measurement	Multiple Observations	M87*: 3 observations within 20 days; Sgr A*: 3 full nights with full array	230+345	No	1
Black Holes & their Cosmic Context												
†Reveal Black Hole-Galaxy Formation, Growth and Coevolution	X	X	X			SMBH masses and indirect estimates of their spins	SMBH emission ring and its polarized structure in a sample of >10 sources	Multiple Observations	One observation (~one night) per target, repeated twice	230	No	1
Determine how SMBHs merge through observations of sub-parsec binaries			X			SMBH binary orbit, masses, and (indirect) spins	SMBH spatial separation & evolution of that spatial separation	Periodic Monitoring	Several measurements taken over at least half of the orbital period (months to years)	230	No	1
Connect SMBHs to high-energy and neutrino events within their jets	X			X	X	Neutrinos produced in regions with PeV protons	Mapping of the jet (imaging), neutrino emission location	Multiple Observations	~Monthly observations of >20 bright blazars and those with neutrino triggers	86+230+345	Yes	1
Black Hole Accretion												
†Reveal how black holes accrete material using resolved movies on event horizon scales	X	X				Accreting plasma properties	Surface brightness and spectral index of the direct image near the photon ring	Periodic Monitoring	M87*: Every 3 days for 3 months (250GM/c³); Sgr A*: One full night at least 3 times	86+230+345 230+345	Yes	M87*: 1 Sgr A*: 2
†Observe localized heating and acceleration of relativistic electrons on astrophysical scales	X	X				Time-dependent temp., |B|, and density in flaring regions	Spatially and time-resolved compact flaring structures in sub-mm movies	Periodic Monitoring	M87*: Every 3 days for 3 months (250GM/c³); Sgr A*: One full night at least 3 times	86+230+345 230+345	Yes	M87*: 1 Sgr A*: 2
Detect frame dragging within the ergosphere of a rotating black hole	X	X				Direction of accretion flow rotation on scales of 2-10M	Radial evolution of resolved polarization structure and dynamics on scales of 2-10M	Periodic Monitoring	M87*: Every 3 days for 3 months (250GM/c³); Sgr A*: One full night at least 3 times	86+230+345 230+345	Yes	2
Jet Launching												
†Determine whether jets are powered by energy extraction from rotating black holes	X					Magnetic flux threading BH, BH spin, and total jet power	Polarized, multi-frequency images on horizon scales and SMBH spin estimate	Multiple Observations	Every 3 days for 3 months (250GM/c³)	86+230+345	Yes	2
†Determine the physical conditions and launching mechanisms for relativistic jets	X					Jet/counter-jet composition, B-field structure, and velocity field on scales of 5-100M	Full polarization, multi-frequency movies with spectral index and rotation measure	Periodic Monitoring	Every 3 days for 3 months (250GM/c³)	86+230	No	1
	X							Multiple Observations	One full night at least 3 times	230+345	Yes	1
Transients												
Measure the inner jet structure and dynamics in black hole X-ray binaries				X	X	Jet collimation profile and velocity at 10⁵-10⁶ M	Motion, brightness, and size of ejected components during flares	Target of Opportunity	Triggered ~10-hr observation with 1-2 follow ups on ~days timescale. 2-4 targets per year	86+230	Yes	1
Detect the kinetic power, physical structure, and velocity in extragalactic transients				X	X	Kinetic power, structure, and velocity of transient outflows	Temporally and spatially resolved morphology of transient outflows	Target of Opportunity	Monthly observations following initial detection for 1-2 years. 2-3 targets per year	86+230	Yes	1
New Horizons												
Detect proper motions and secular (CMB) parallaxes of AGN up to ~80 Mpc distances					X	Proper motions and secular (CMB) parallaxes	Multi-year tracking of many sources across the sky with 1ps (~5 μs) delay fidelity	Multiple Observations	Multiple observations spread over >3 years per source for >10 sources	86+230	Yes	2
Leverage AGN accretion disk megamasers to measure their AGN host properties					X	SMBH masses and distances; Hubble constant	Spectral lines of megamasers	Multiple Observations	Monthly observations of ~10 sources	300-325	No	1

Figure 12. Representative subset of the ngEHT Science Traceability Matrix (STM). Daggers (†) indicate threshold science goals. The STM is used to guide the array design and to inform decisions about the multi-phase deployment.

In conclusion, the ngEHT scientific community has identified a series of science objectives, with associated observational advances that are feasible over the coming decade. Taken together, they offer a remarkable opportunity to push the frontiers of VLBI and to enable a series of new discoveries that will elucidate the extraordinary role of BHs across all astrophysical scales.

Author Contributions: Conceptualization, M.D.J.; software, A.E.B., M.D.J. and D.W.P.; writing—original draft preparation, M.D.J., L.B., V.C., R.P.F., C.M.F., P.G., J.L.G., D.H., M.L.L., A.P.L., S.M., R.N., P.N., D.W.P., Z.Y., K.C., J.D., R.D., J.E., Y.Y.K., R.L., A.M., N.C.M.M., N.M.N., D.C.M.P., A.R., M.J.R., F.R. and A.C.T.; writing—review and editing, M.D.J., L.B., V.C., R.P.F., C.M.F., P.G., J.L.G., D.H., M.L.L., A.P.L., S.M., R.N., P.N., T.N., D.W.P., Z.Y., K.C., J.D., R.D., S.S.D., J.E., G.F., S.I., Y.Y.K., R.L., A.M., N.C.M.M., N.M.N., D.C.M.P., A.R., M.J.R., F.R., A.C.T., P.T., K.A., K.L.B., A.C., R.C., K.H.,

Notes

1. Since its first observing campaign, three sites have joined the EHT (see Figure 1). These additions are expected to substantially improve upon the dynamic range of published EHT images.
2. In contrast, most telescopes of the present EHT are astronomical facilities that only commit a small fraction of their total observing time to VLBI.
3. https://www.ngeht.org/ngeht-meeting-2021 (accessed on 20 April 2023).
4. https://www.ngeht.org/ngeht-meeting-november-2021 (accessed on 20 April 2023).
5. https://www.ngeht.org/ngeht-meeting-june-2022 (accessed on 20 April 2023).
6. https://www.ngeht.org/broadening-horizons-2022 (accessed on 20 April 2023).
7. https://www.mdpi.com/journal/galaxies/special_issues/ngEHT_blackholes (accessed on 20 April 2023).
8. Angular momentum transport may also occur in magnetic flux eruptions (see, e.g., [151]), which would also have distinctive signatures in ngEHT images and movies (see, e.g., [102,152,153]).
9. https://challenge.ngeht.org/ (accessed on 20 April 2023).
10. Two excellent doctoral dissertations offer fine-grained analysis of the mountaintop dispute, and are a good entry point into this issue. Ref. [249] focuses on the triply conflicting astronomical, environmental and indigenous narratives that collided at Mt. Graham, Mauna Kea, and Kitt Peak; Ref. [250] addresses the Kanaka rights claim, specifically about the Thirty Meter Telescope (TMT), in opposition to a framing of the dispute as one of "stakeholders" or a "multicultural" ideal. Ref. [251] focuses on Mauna Kea in a subsequent article, also on the TMT. An important current Hawaiian-led impact assessment of the TMT, including further links, is [252]; other Native Hawaiian scientists, including [253] have spoken for a much-changed process and against the notion that opposition to the TMT is against science.
11. The workshop was held on the 4th of November 2022. Workshop Speakers included C. Prescod-Weinstein, K. Kamelamela, H. Nielson, M. Johnson, J. Havstad, T. Nichols, R. Chiaravalloti, S. Doeleman, G. Fitzpatrick, J. Houston, A. Oppenheimer, P. Galison, A. Thresher and P. Natarajan. Much of the work being performed by the responsible siting group owes its genesis in the excellent contributions of the speakers and attendees of the workshop and we are grateful for their past and ongoing contributions.
12. For a detailed discussion of siting and community guidelines for gene-drive technology, for example, see Singh [254].

13　There is much discussion within these fields of how we ought to think about community-led and non-extractive science. Good starting places for the literature include Watkins [255], Supernant and Warrick [256].

14　An outstanding example of joint concern crossing environmental, cultural, epistemic, and technical concerns, in the case of LIGO, can be found in Nichols [257]. Another instanced of community participation by (here in relation to NASA for their Asteroid Redirect Mission): Tomblin et al. [258]. On the siting of the Superconducting Supercollider, Riordan et al. [259]; an historical-anthropological study of the placement of the French/European launch center, Redfield [260].

15　Consent, and environmental justice, have been at the center of siting nuclear facilities, including power generation, weapons testing, accident sites, and waste disposal. The literature is vast, but a starting point with many further references can be found in sources including: Gerrard [261] addresses community concerns about siting from the perspective on an environmental lawyer; Kuletz [262] focuses on Western US nuclear sites of waste; Masco [263] attends to the quadruple intersection of weapons scientists, Pueblo Indian nations, nuevomexicano communities, and activists as they live amidst and confront the legacy of Los Alamos. On consent-based siting rather than top-down imposition, see Hamilton et al. [264]; and for a recent development and analysis of consent-based siting, Richter et al. [265].

16　For lessons learnt regarding knowledge formation, governance, organisational structure, decision-making, diversity, account-ability, creativity, credit assignment and the role of consensus, from a range of perspectives across the humanities and social sciences, see e.g., (a) in general: Galison and Hevly [272], Knorr Cetina [273], Sullivan [274], Shrum et al. [275], Boyer-Kassem et al. [276] and references therein; (b) for specific collaborations and institutions: Collins [277], Nichols [278] on LIGO; Boisot et al. [279], Ritson [280], Sorgner [281], Merz and Sorgner [282] on ATLAS and/or CERN; Jebeile [283] on the IPCC; Smith et al. [284], Vertesi [285] on NASA; and Traweek [286] on SLAC and KEK.

17　Regarding network analysis, communication structures and epistemic communities, see for instance the following texts and references therein: Kitcher [290,291], Zollman [292,293,294], Longino [295], Lalli et al. [296,297], Light and Moody [298], Wüthrich [299], Šešelja [300].

18　Regarding authorship challenges and possible solutions relevant to the ngEHT context, see e.g., Resnik [301], Boyer-Kassem et al. [276], Rennie et al. [302], Cronin [303], Galison [304], Wray [305], McNutt et al. [306], Bright et al. [307], Heesen [308], Dang [309], Nogrady [310], Habgood-Coote [311] and www.icmje.org/icmje-recommendations.pdf (accessed on 20 April 2023).

References

1. Akiyama, K. et al. [Event Horizon Telescope Collaboration]. First M87 Event Horizon Telescope Results. I. The Shadow of the Supermassive Black Hole. *Astrophys. J. Lett.* **2019**, *875*, L1. [CrossRef]
2. Akiyama, K. et al. [Event Horizon Telescope Collaboration]. First M87 Event Horizon Telescope Results. II. Array and Instrumentation. *Astrophys. J. Lett.* **2019**, *875*, L2. [CrossRef]
3. Akiyama, K. et al. [Event Horizon Telescope Collaboration]. First M87 Event Horizon Telescope Results. III. Data Processing and Calibration. *Astrophys. J. Lett.* **2019**, *875*, L3. [CrossRef]
4. Akiyama, K. et al. [Event Horizon Telescope Collaboration]. First M87 Event Horizon Telescope Results. IV. Imaging the Central Supermassive Black Hole. *Astrophys. J. Lett.* **2019**, *875*, L4. [CrossRef]
5. Akiyama, K. et al. [Event Horizon Telescope Collaboration]. First M87 Event Horizon Telescope Results. V. Physical Origin of the Asymmetric Ring. *Astrophys. J. Lett.* **2019**, *875*, L5. [CrossRef]
6. Akiyama, K. et al. [Event Horizon Telescope Collaboration]. First M87 Event Horizon Telescope Results. VI. The Shadow and Mass of the Central Black Hole. *Astrophys. J. Lett.* **2019**, *875*, L6. [CrossRef]
7. Akiyama, K. et al. [Event Horizon Telescope Collaboration]. First M87 Event Horizon Telescope Results. VII. Polarization of the Ring. *Astrophys. J. Lett.* **2021**, *910*, L12. [CrossRef]
8. Akiyama, K. et al. [Event Horizon Telescope Collaboration]. First M87 Event Horizon Telescope Results. VIII. Magnetic Field Structure near The Event Horizon. *Astrophys. J. Lett.* **2021**, *910*, L13. [CrossRef]
9. Akiyama, K. et al. [Event Horizon Telescope Collaboration]. First Sagittarius A* Event Horizon Telescope Results. I. The Shadow of the Supermassive Black Hole in the Center of the Milky Way. *Astrophys. J. Lett.* **2022**, *930*, L12. [CrossRef]
10. Akiyama, K. et al. [Event Horizon Telescope Collaboration]. First Sagittarius A* Event Horizon Telescope Results. II. EHT and Multiwavelength Observations, Data Processing, and Calibration. *Astrophys. J. Lett.* **2022**, *930*, L13. [CrossRef]
11. Akiyama, K. et al. [Event Horizon Telescope Collaboration]. First Sagittarius A* Event Horizon Telescope Results. III. Imaging of the Galactic Center Supermassive Black Hole. *Astrophys. J. Lett.* **2022**, *930*, L14. [CrossRef]
12. Akiyama, K. et al. [Event Horizon Telescope Collaboration]. First Sagittarius A* Event Horizon Telescope Results. IV. Variability, Morphology, and Black Hole Mass. *Astrophys. J. Lett.* **2022**, *930*, L15. . [CrossRef]
13. Akiyama, K. et al. [Event Horizon Telescope Collaboration]. First Sagittarius A* Event Horizon Telescope Results. V. Testing Astrophysical Models of the Galactic Center Black Hole. *Astrophys. J. Lett.* **2022**, *930*, L16. [CrossRef]
14. Akiyama, K. et al. [Event Horizon Telescope Collaboration]. First Sagittarius A* Event Horizon Telescope Results. VI. Testing the Black Hole Metric. *Astrophys. J. Lett.* **2022**, *930*, L17. [CrossRef]
15. Algaba, J.C. et al. [EHT MWL Science Working Group]. Broadband Multi-wavelength Properties of M87 during the 2017 Event Horizon Telescope Campaign. *Astrophys. J. Lett.* **2021**, *911*, L11. [CrossRef]

16. Kim, J.Y.; Krichbaum, T.P.; Broderick, A.E.; Wielgus, M.; Blackburn, L.; Gómez, J.L.; Johnson, M.D.; Bouman, K.L.; Chael, A.; Akiyama, K.; et al. Event Horizon Telescope imaging of the archetypal blazar 3C 279 at an extreme 20 microarcsecond resolution. *Astron. Astrophys.* **2020**, *640*, A69. [CrossRef]

17. Janssen, M.; Falcke, H.; Kadler, M.; Ros, E.; Wielgus, M.; Akiyama, K.; Baloković, M.; Blackburn, L.; Bouman, K.L.; Chael, A.; et al. Event Horizon Telescope observations of the jet launching and collimation in Centaurus A. *Nat. Astron.* **2021**, *5*, 1017–1028. [CrossRef]

18. Issaoun, S.; Wielgus, M.; Jorstad, S.; Krichbaum, T.P.; Blackburn, L.; Janssen, M.; Chan, C.k.; Pesce, D.W.; Gómez, J.L.; Akiyama, K.; et al. Resolving the Inner Parsec of the Blazar J1924-2914 with the Event Horizon Telescope. *Astrophys. J. Suppl.* **2022**, *934*, 145. [CrossRef]

19. Jorstad, S.; Wielgus, M.; Lico, R.; Issaoun, S.; Broderick, A.E.; Pesce, D.W.; Liu, J.; Zhao, G.Y.; Krichbaum, T.P.; Blackburn, L.; et al. The Event Horizon Telescope Image of the Quasar NRAO 530. *Astrophys. J. Suppl.* **2023**, *943*, 170. [CrossRef]

20. Thompson, A.R.; Moran, J.M.; Swenson, G.W. *Interferometry and Synthesis in Radio Astronomy*, 3rd ed.; Springer: Berlin/Heidelberg, Germany, 2017. [CrossRef]

21. Padin, S.; Woody, D.P.; Hodges, M.W.; Rogers, A.E.E.; Emerson, D.T.; Jewell, P.R.; Lamb, J.; Perfetto, A.; Wright, M.C.H. 223 GHz VLBI Observations of 3C 273. *Astrophys. J. Lett.* **1990**, *360*, L11. [CrossRef]

22. Krichbaum, T.P.; Graham, D.A.; Witzel, A.; Greve, A.; Wink, J.E.; Grewing, M.; Colomer, F.; de Vicente, P.; Gomez-Gonzalez, J.; Baudry, A.; et al. VLBI observations of the galactic center source SGR A* at 86 GHz and 215 GHz. *Astron. Astrophys.* **1998**, *335*, L106–L110.

23. Doeleman, S.S.; Weintroub, J.; Rogers, A.E.E.; Plambeck, R.; Freund, R.; Tilanus, R.P.J.; Friberg, P.; Ziurys, L.M.; Moran, J.M.; Corey, B.; et al. Event-horizon-scale structure in the supermassive black hole candidate at the Galactic Centre. *Nature* **2008**, *455*, 78–80. [CrossRef]

24. Boccardi, B.; Krichbaum, T.P.; Ros, E.; Zensus, J.A. Radio observations of active galactic nuclei with mm-VLBI. *Astron. Astrophys. Rev.* **2017**, *25*, 4. [CrossRef]

25. Bardeen, J.M. Timelike and null geodesics in the Kerr metric. In *Black Holes (Les Astres Occlus)*; Gordon and Breach: New York, NY, USA, 1973; pp. 215–239.

26. Luminet, J.P. Image of a spherical black hole with thin accretion disk. *Astron. Astrophys.* **1979**, *75*, 228–235.

27. Falcke, H.; Melia, F.; Agol, E. Viewing the Shadow of the Black Hole at the Galactic Center. *Astrophys. J. Lett.* **2000**, *528*, L13–L16. [CrossRef] [PubMed]

28. de Vries, A. The apparent shape of a rotating charged black hole, closed photon orbits and the bifurcation set A_4. *Class. Quant. Gravity* **2000**, *17*, 123–144. [CrossRef]

29. Mościbrodzka, M.; Dexter, J.; Davelaar, J.; Falcke, H. Faraday rotation in GRMHD simulations of the jet launching zone of M87. *Mon. Not. RAS* **2017**, *468*, 2214–2221. [CrossRef]

30. Ricarte, A.; Prather, B.S.; Wong, G.N.; Narayan, R.; Gammie, C.; Johnson, M.D. Decomposing the internal faraday rotation of black hole accretion flows. *Mon. Not. RAS* **2020**, *498*, 5468–5488. [CrossRef]

31. Chael, A.; Issaoun, S.; Pesce, D.W.; Johnson, M.D.; Ricarte, A.; Fromm, C.M.; Mizuno, Y. Multi-frequency Black Hole Imaging for the Next-Generation Event Horizon Telescope. *arXiv* **2022**, arXiv:2210.12226.

32. Ricarte, A.; Johnson, M.D.; Kovalev, Y.Y.; Palumbo, D.C.M.; Emami, R. How Spatially Resolved Polarimetry Informs Black Hole Accretion Flow Models. *Galaxies* **2023**, *11*, 5. [CrossRef]

33. Crew, G.B.; Goddi, C.; Matthews, L.D.; Rottmann, H.; Saez, A.; Martí-Vidal, I. A Characterization of the ALMA Phasing System at 345 GHz. *Publ. ASP* **2023**, *135*, 025002. [CrossRef]

34. Roelofs, F.; Blackburn, L.; Lindahl, G.; Doeleman, S.S.; Johnson, M.D.; Arras, P.; Chatterjee, K.; Emami, R.; Fromm, C.; Fuentes, A.; et al. The ngEHT Analysis Challenges. *Galaxies* **2023**, *11*, 12. [CrossRef]

35. Walker, R.C.; Hardee, P.E.; Davies, F.B.; Ly, C.; Junor, W. The Structure and Dynamics of the Subparsec Jet in M87 Based on 50 VLBA Observations over 17 Years at 43 GHz. *Astrophys. J.* **2018**, *855*, 128. [CrossRef]

36. Wielgus, M.; Akiyama, K.; Blackburn, L.; Chan, C.K.; Dexter, J.; Doeleman, S.S.; Fish, V.L.; Issaoun, S.; Johnson, M.D.; Krichbaum, T.P.; et al. Monitoring the Morphology of M87* in 2009–2017 with the Event Horizon Telescope. *Astrophys. J.* **2020**, *901*, 67. [CrossRef]

37. Raymond, A.W.; Palumbo, D.; Paine, S.N.; Blackburn, L.; Córdova Rosado, R.; Doeleman, S.S.; Farah, J.R.; Johnson, M.D.; Roelofs, F.; Tilanus, R.P.J.; et al. Evaluation of New Submillimeter VLBI Sites for the Event Horizon Telescope. *Astrophys. J. Suppl.* **2021**, *253*, 5. [CrossRef]

38. Bustamante, S.; Blackburn, L.; Narayanan, G.; Schloerb, F.P.; Hughes, D. The Role of the Large Millimeter Telescope in Black Hole Science with the Next-Generation Event Horizon Telescope. *Galaxies* **2023**, *11*, 2. [CrossRef]

39. Yu, W.; Lu, R.S.; Shen, Z.Q.; Weintroub, J. Evaluation of a Candidate Site in the Tibetan Plateau towards the Next Generation Event Horizon Telescope. *Galaxies* **2023**, *11*, 7. [CrossRef]

40. Akiyama, K.; Kauffmann, J.; Matthews, L.D.; Moriyama, K.; Koyama, S.; Hada, K. Millimeter/Submillimeter VLBI with a Next Generation Large Radio Telescope in the Atacama Desert. *Galaxies* **2023**, *11*, 1. [CrossRef]

41. Kauffmann, J.; Rajagopalan, G.; Akiyama, K.; Fish, V.; Lonsdale, C.; Matthews, L.D.; Pillai, T.G. The Haystack Telescope as an Astronomical Instrument. *Galaxies* **2023**, *11*, 9. [CrossRef]

42. Asada, K.; Kino, M.; Honma, M.; Hirota, T.; Lu, R.S.; Inoue, M.; Sohn, B.W.; Shen, Z.Q.; Ho, P.T.P.; Akiyama, K.; et al. White Paper on East Asian Vision for mm/submm VLBI: Toward Black Hole Astrophysics down to Angular Resolution of 1_S. *arXiv* **2017**, arXiv:1705.04776.

43. Backes, M.; Müller, C.; Conway, J.E.; Deane, R.; Evans, R.; Falcke, H.; Fraga-Encinas, R.; Goddi, C.; Klein Wolt, M.; Krichbaum, T.P.; et al. The Africa Millimetre Telescope. In Proceedings of the 4th Annual Conference on High Energy Astrophysics in Southern Africa (HEASA 2016), Cape Town, South Africa, 25–27 August 2016; p. 29. [CrossRef]

44. Romero, G.E. Large Latin American Millimeter Array. *arXiv* **2020**, arXiv:2010.00738.

45. Issaoun, S.; Pesce, D.W.; Roelofs, F.; Chael, A.; Dodson, R.; Rioja, M.J.; Akiyama, K.; Aran, R.; Blackburn, L.; Doeleman, S.S.; et al. Enabling Transformational ngEHT Science via the Inclusion of 86 GHz Capabilities. *Galaxies* **2023**, *11*, 28. [CrossRef]

46. Rioja, M.J.; Dodson, R.; Asaki, Y. The Transformational Power of Frequency Phase Transfer Methods for ngEHT. *Galaxies* **2023**, *11*, 16. [CrossRef]

47. Jiang, W.; Zhao, G.Y.; Shen, Z.Q.; Rioja, M.J.; Dodson, R.; Cho, I.; Zhao, S.S.; Eubanks, M.; Lu, R.S. Applications of the Source-Frequency Phase-Referencing Technique for ngEHT Observations. *Galaxies* **2023**, *11*, 3. [CrossRef]

48. Doeleman, S.; Blackburn, L.; Dexter, J.; Gomez, J.L.; Johnson, M.D.; Palumbo, D.C.; Weintroub, J.; Farah, J.R.; Fish, V.; Loinard, L.; et al. Studying Black Holes on Horizon Scales with VLBI Ground Arrays. *Bull. Am. Astron. Soc.* **2019**, *51*, 256.

49. Inoue, M.; Algaba-Marcos, J.C.; Asada, K.; Blundell, R.; Brisken, W.; Burgos, R.; Chang, C.C.; Chen, M.T.; Doeleman, S.S.; Fish, V.; et al. Greenland telescope project: Direct confirmation of black hole with sub-millimeter VLBI. *Radio Sci.* **2014**, *49*, 564–571. [CrossRef]

50. Doeleman, S. et al. [ngEHT Collaboration]. Reference Array and Design Consideration for the next-generation Event Horizon Telescope. *Galaxies* **2023**, *in prepration*.

51. Selina, R.J.; Murphy, E.J.; McKinnon, M.; Beasley, A.; Butler, B.; Carilli, C.; Clark, B.; Durand, S.; Erickson, A.; Grammer, W.; et al. The ngVLA Reference Design. In *Science with a Next Generation Very Large Array*; Murphy, E., Ed.; Astronomical Society of the Pacific Conference Series; NASA/ADS: Cambridge, MA, USA, 2018; Volume 517, p. 15,

52. Galison, P.; Doboszewski, J.; Elder, J.; Martens, N.C.M.; Ashtekar, A.; Enander, J.; Gueguen, M.; Kessler, E.A.; Lalli, R.; Lesourd, M.; et al. The Next Generation Event Horizon Telescope Collaboration: History, Philosophy, and Culture. *Galaxies* **2023**, *11*, 32. [CrossRef]

53. Penrose, R. Gravitational Collapse: the Role of General Relativity. *Nuovo Cim. Riv. Ser.* **1969**, *1*, 252.

54. Shakura, N.I.; Sunyaev, R.A. Black holes in binary systems. Observational appearance. *Astron. Astrophys.* **1973**, *24*, 337–355.

55. Blandford, R.D.; Znajek, R.L. Electromagnetic extraction of energy from Kerr black holes. *Mon. Not. RAS* **1977**, *179*, 433–456. [CrossRef]

56. Yuan, F.; Narayan, R. Hot Accretion Flows Around Black Holes. *Ann. Rev. Astron. Astrophys.* **2014**, *52*, 529–588. [CrossRef]

57. Harlow, D. Jerusalem lectures on black holes and quantum information. *Revi. Modern Phys.* **2016**, *88*, 015002. [CrossRef]

58. Senovilla, J.M.M.; Garfinkle, D. The 1965 Penrose singularity theorem. *Class. Quant. Gravity* **2015**, *32*, 124008. [CrossRef]

59. Chael, A.; Johnson, M.D.; Lupsasca, A. Observing the Inner Shadow of a Black Hole: A Direct View of the Event Horizon. *Astrophys. J.* **2021**, *918*, 6. [CrossRef]

60. Johnson, M.D.; Lupsasca, A.; Strominger, A.; Wong, G.N.; Hadar, S.; Kapec, D.; Narayan, R.; Chael, A.; Gammie, C.F.; Galison, P.; et al. Universal interferometric signatures of a black hole's photon ring. *Sci. Adv.* **2020**, *6*, eaaz1310. [CrossRef]

61. Ayzenberg, D.; Brito, R.; Britzen, S.; Broderick, A.E.; Carballo-Rubio, R.; Cardoso, V.; Chael, A.; Chen, Y.; Cunha, P.V.P.; Eichhorn, A.; et al. Fundamental Physics Opportunities with the Next-Generation Event Horizon Telescope. 2023. Available online: https://www.ngeht.org/hpc (accessed on 20 April 2023).

62. Carballo-Rubio, R.; Di Filippo, F.; Liberati, S.; Visser, M. Phenomenological aspects of black holes beyond general relativity. *Phys. Rev. D* **2018**, *98*, 124009. [CrossRef]

63. Cardoso, V.; Pani, P. Testing the nature of dark compact objects: A status report. *Liv. Rev. Relat.* **2019**, *22*, 4. [CrossRef]

64. Jaroszynski, M.; Kurpiewski, A. Optics near Kerr black holes: spectra of advection dominated accretion flows. *Astron. Astrophys.* **1997**, *326*, 419–426. [CrossRef]

65. Narayan, R.; Johnson, M.D.; Gammie, C.F. The Shadow of a Spherically Accreting Black Hole. *Astrophys. J. Lett.* **2019**, *885*, L33. [CrossRef]

66. Younsi, Z.; Psaltis, D.; Özel, F. Black Hole Images as Tests of General Relativity: Effects of Spacetime Geometry. *Astrophys. J.* **2023**, *942*, 47. [CrossRef]

67. Dokuchaev, V.I.; Nazarova, N.O. Event Horizon Image within Black Hole Shadow. *Sov. J. Exp. Theor. Phys.* **2019**, *128*, 578–585. [CrossRef]

68. Psaltis, D.; Medeiros, L.; Christian, P.; Özel, F.; Akiyama, K.; Alberdi, A.; Alef, W.; Asada, K.; Azulay, R.; Ball, D.; et al. Gravitational Test beyond the First Post-Newtonian Order with the Shadow of the M87 Black Hole. *Phys. Rev. Lett.* **2020**, *125*, 141104. [CrossRef]

69. Kocherlakota, P.; Rezzolla, L.; Falcke, H.; Fromm, C.M.; Kramer, M.; Mizuno, Y.; Nathanail, A.; Olivares, H.; Younsi, Z.; Akiyama, K.; et al. Constraints on black-hole charges with the 2017 EHT observations of M87*. *Phys. Rev. D* **2021**, *103*, 104047. [CrossRef]

70. Vincent, F.H.; Wielgus, M.; Abramowicz, M.A.; Gourgoulhon, E.; Lasota, J.P.; Paumard, T.; Perrin, G. Geometric modeling of M87* as a Kerr black hole or a non-Kerr compact object. *Astron. Astrophys.* **2021**, *646*, A37. [CrossRef]

71. Carballo-Rubio, R.; Cardoso, V.; Younsi, Z. Toward very large baseline interferometry observations of black hole structure. *Phys. Rev. D* **2022**, *106*, 084038. [CrossRef]

72. Abuter, R. et al. [GRAVITY Collaboration]. Mass distribution in the Galactic Center based on interferometric astrometry of multiple stellar orbits. *Astron. Astrophys.* **2022**, *657*, L12. [CrossRef]

73. Do, T.; Hees, A.; Ghez, A.; Martinez, G.D.; Chu, D.S.; Jia, S.; Sakai, S.; Lu, J.R.; Gautam, A.K.; O'Neil, K.K.; et al. Relativistic redshift of the star S0-2 orbiting the Galactic Center supermassive black hole. *Science* **2019**, *365*, 664–668. [CrossRef] [PubMed]

74. Takahashi, R. Shapes and Positions of Black Hole Shadows in Accretion Disks and Spin Parameters of Black Holes. *Astrophys. J.* **2004**, *611*, 996–1004. [CrossRef]

75. Tiede, P. Comrade: Composable Modeling of Radio Emission. *J. Open Source Softw.* **2022**, *7*, 4457. [CrossRef]

76. Robinson, D.C. Uniqueness of the Kerr Black Hole. *Phys. Rev. Lett.* **1975**, *34*, 905–906. . [CrossRef]

77. Gibbons, G.W. Vacuum polarization and the spontaneous loss of charge by black holes. *Commun. Math. Phys.* **1975**, *44*, 245–264. [CrossRef]

78. Reynolds, C.S. Observational Constraints on Black Hole Spin. *Ann. Rev. Astron. Astrophys.* **2021**, *59*, 117–154. [CrossRef]

79. Ricarte, A.; Tiede, P.; Emami, R.; Tamar, A.; Natarajan, P. The ngEHT's Role in Measuring Supermassive Black Hole Spins. *Galaxies* **2022**, *11*, 6. [CrossRef]

80. Palumbo, D.C.M.; Wong, G.N.; Prather, B.S. Discriminating Accretion States via Rotational Symmetry in Simulated Polarimetric Images of M87. *Astrophys. J.* **2020**, *894*, 156. [CrossRef]

81. Qiu, R.; Ricarte, A.; Narayan, R.; Wong, G.N.; Chael, A.; Palumbo, D. Using Machine Learning to Link Black Hole Accretion Flows with Spatially Resolved Polarimetric Observables. *arXiv* **2022**, arXiv:2212.04852.

82. Palumbo, D.C.M.; Gelles, Z.; Tiede, P.; Chang, D.O.; Pesce, D.W.; Chael, A.; Johnson, M.D. Bayesian Accretion Modeling: Axisymmetric Equatorial Emission in the Kerr Spacetime. *Astrophys. J.* **2022**, *939*, 107. [CrossRef]

83. Jiménez-Rosales, A.; Dexter, J.; Ressler, S.M.; Tchekhovskoy, A.; Bauböck, M.; Dallilar, Y.; de Zeeuw, P.T.; Drescher, A.; Eisenhauer, F.; von Fellenberg, S.; et al. Relative depolarization of the black hole photon ring in GRMHD models of Sgr A* and M87*. *Mon. Not. RAS* **2021**, *503*, 4563–4575. [CrossRef]

84. Palumbo, D.C.M.; Wong, G.N. Photon Ring Symmetries in Simulated Linear Polarization Images of Messier 87*. *Astrophys. J.* **2022**, *929*, 49. [CrossRef]

85. Palumbo, D.P. Spin Signatures of Rotating Black Holes. 2023.

86. Teo, E. Spherical Photon Orbits Around a Kerr Black Hole. *Gener. Relat. Gravit.* **2003**, *35*, 1909–1926. .:1026286607562. [CrossRef]

87. Tiede, P.; Johnson, M.D.; Pesce, D.W.; Palumbo, D.C.M.; Chang, D.O.; Galison, P. Measuring Photon Rings with the ngEHT. *Galaxies* **2022**, *10*, 111. [CrossRef]

88. Johannsen, T.; Psaltis, D. Testing the No-hair Theorem with Observations in the Electromagnetic Spectrum. II. Black Hole Images. *Astrophys. J.* **2010**, *718*, 446–454. [CrossRef]

89. Wielgus, M. Photon rings of spherically symmetric black holes and robust tests of non-Kerr metrics. *Phys. Rev. D* **2021**, *104*, 124058. [CrossRef]

90. Broderick, A.E.; Tiede, P.; Pesce, D.W.; Gold, R. Measuring Spin from Relative Photon-ring Sizes. *Astrophys. J.* **2022**, *927*, 6. [CrossRef]

91. Psaltis, D.; Johnson, M.; Narayan, R.; Medeiros, L.; Blackburn, L.; Bower, G. A Model for Anisotropic Interstellar Scattering and its Application to Sgr A*. *arXiv* **2018**, arXiv:1805.01242.

92. Johnson, M.D.; Narayan, R.; Psaltis, D.; Blackburn, L.; Kovalev, Y.Y.; Gwinn, C.R.; Zhao, G.Y.; Bower, G.C.; Moran, J.M.; Kino, M.; et al. The Scattering and Intrinsic Structure of Sagittarius A* at Radio Wavelengths. *Astrophys. J.* **2018**, *865*, 104. [CrossRef]

93. Issaoun, S.; Johnson, M.D.; Blackburn, L.; Brinkerink, C.D.; Mościbrodzka, M.; Chael, A.; Goddi, C.; Martí-Vidal, I.; Wagner, J.; Doeleman, S.S.; et al. The Size, Shape, and Scattering of Sagittarius A* at 86 GHz: First VLBI with ALMA. *Astrophys. J.* **2019**, *871*, 30. [CrossRef]

94. Zhu, Z.; Johnson, M.D.; Narayan, R. Testing General Relativity with the Black Hole Shadow Size and Asymmetry of Sagittarius A*: Limitations from Interstellar Scattering. *Astrophys. J.* **2019**, *870*, 6. [CrossRef]

95. Broderick, A.E.; Loeb, A. Imaging optically-thin hotspots near the black hole horizon of Sgr A* at radio and near-infrared wavelengths. *Mon. Not. RAS* **2006**, *367*, 905–916. [CrossRef]

96. Moriyama, K.; Mineshige, S.; Honma, M.; Akiyama, K. Black Hole Spin Measurement Based on Time-domain VLBI Observations of Infalling Gas Clouds. *Astrophys. J.* **2019**, *887*, 227. [CrossRef]

97. Tiede, P.; Pu, H.Y.; Broderick, A.E.; Gold, R.; Karami, M.; Preciado-López, J.A. Spacetime Tomography Using the Event Horizon Telescope. *Astrophys. J.* **2020**, *892*, 132. [CrossRef]

98. Chesler, P.M.; Blackburn, L.; Doeleman, S.S.; Johnson, M.D.; Moran, J.M.; Narayan, R.; Wielgus, M. Light echos and coherent autocorrelations in a black hole spacetime. *Class. Quant. Gravity* **2021**, *38*, 125006. [CrossRef]

99. Hadar, S.; Johnson, M.D.; Lupsasca, A.; Wong, G.N. Photon ring autocorrelations. *Phys. Rev. D* **2021**, *103*, 104038. [CrossRef]

100. Wong, G.N. Black Hole Glimmer Signatures of Mass, Spin, and Inclination. *Astrophys. J.* **2021**, *909*, 217. [CrossRef]

101. Gelles, Z.; Himwich, E.; Johnson, M.D.; Palumbo, D.C.M. Polarized image of equatorial emission in the Kerr geometry. *Phys. Rev. D* **2021**, *104*, 044060. [CrossRef]

102. Gelles, Z.; Chatterjee, K.; Johnson, M.; Ripperda, B.; Liska, M. Relativistic Signatures of Flux Eruption Events near Black Holes. *Galaxies* **2022**, *10*, 107. [CrossRef]

103. Wielgus, M.; Moscibrodzka, M.; Vos, J.; Gelles, Z.; Martí-Vidal, I.; Farah, J.; Marchili, N.; Goddi, C.; Messias, H. Orbital motion near Sagittarius A* . Constraints from polarimetric ALMA observations. *Astron. Astrophys.* **2022**, *665*, L6. [CrossRef]

104. Vos, J.; Mościbrodzka, M.A.; Wielgus, M. Polarimetric signatures of hot spots in black hole accretion flows. *Astron. Astrophys.* **2022**, *668*, A185. [CrossRef]

105. Emami, R.; Tiede, P.; Doeleman, S.S.; Roelofs, F.; Wielgus, M.; Blackburn, L.; Liska, M.; Chatterjee, K.; Ripperda, B.; Fuentes, A.; et al. Tracing Hot Spot Motion in Sagittarius A* Using the Next-Generation Event Horizon Telescope (ngEHT). *Galaxies* **2023**, *11*, 23. [CrossRef]

106. Peccei, R.D.; Quinn, H.R. Constraints imposed by CP conservation in the presence of pseudoparticles. *Phys. Rev. D* **1977**, *16*, 1791–1797. [CrossRef]

107. Preskill, J.; Wise, M.B.; Wilczek, F. Cosmology of the invisible axion. *Phys. Lett. B* **1983**, *120*, 127–132. [CrossRef]

108. Abbott, L.F.; Sikivie, P. A cosmological bound on the invisible axion. *Phys. Lett. B* **1983**, *120*, 133–136. [CrossRef]

109. Dine, M.; Fischler, W. The not-so-harmless axion. *Phys. Lett. B* **1983**, *120*, 137–141. [CrossRef]

110. Arvanitaki, A.; Dimopoulos, S.; Dubovsky, S.; Kaloper, N.; March-Russell, J. String Axiverse. *Phys. Rev. D* **2010**, *81*, 123530. [CrossRef]

111. Brito, R.; Cardoso, V.; Pani, P. Superradiance: New Frontiers in Black Hole Physics. *Lect. Notes Phys.* **2015**, *906*, 1–237. [CrossRef]

112. Hu, W.; Barkana, R.; Gruzinov, A. Cold and fuzzy dark matter. *Phys. Rev. Lett.* **2000**, *85*, 1158–1161. [CrossRef] [PubMed]

113. Davoudiasl, H.; Denton, P.B. Ultralight Boson Dark Matter and Event Horizon Telescope Observations of M 87*. *Phys. Rev. Lett.* **2019**, *123*, 021102. [CrossRef] [PubMed]

114. Chen, Y.; Shu, J.; Xue, X.; Yuan, Q.; Zhao, Y. Probing Axions with Event Horizon Telescope Polarimetric Measurements. *Phys. Rev. Lett.* **2020**, *124*, 061102. [CrossRef] [PubMed]

115. Chen, Y.; Liu, Y.; Lu, R.S.; Mizuno, Y.; Shu, J.; Xue, X.; Yuan, Q.; Zhao, Y. Stringent axion constraints with Event Horizon Telescope polarimetric measurements of M87*. *Nat. Astron.* **2022**, *6*, 592–598. [CrossRef]

116. Chen, Y.; Li, C.; Mizuno, Y.; Shu, J.; Xue, X.; Yuan, Q.; Zhao, Y.; Zhou, Z. Birefringence tomography for axion cloud. *J. Cosmol. Aatrop. Phys.* **2022**, *2022*, 073. [CrossRef]

117. Kulier, A.; Ostriker, J.P.; Natarajan, P.; Lackner, C.N.; Cen, R. Understanding Black Hole Mass Assembly via Accretion and Mergers at Late Times in Cosmological Simulations. *Astrophys. J.* **2015**, *799*, 178. [CrossRef]

118. Weinberger, R.; Springel, V.; Pakmor, R.; Nelson, D.; Genel, S.; Pillepich, A.; Vogelsberger, M.; Marinacci, F.; Naiman, J.; Torrey, P.; et al. Supermassive black holes and their feedback effects in the IllustrisTNG simulation. *Mon. Not. RAS* **2018**, *479*, 4056–4072. [CrossRef]

119. Ricarte, A.; Natarajan, P. Exploring SMBH assembly with semi-analytic modelling. *Mon. Not. RAS* **2018**, *474*, 1995–2011. [CrossRef]

120. Pacucci, F.; Loeb, A. Separating Accretion and Mergers in the Cosmic Growth of Black Holes with X-ray and Gravitational-wave Observations. *Astrophys. J.* **2020**, *895*, 95. [CrossRef]

121. Haehnelt, M.G.; Natarajan, P.; Rees, M.J. High-redshift galaxies, their active nuclei and central black holes. *Mon. Not. RAS* **1998**, *300*, 817–827. [CrossRef]

122. Di Matteo, T.; Springel, V.; Hernquist, L. Energy input from quasars regulates the growth and activity of black holes and their host galaxies. *Nature* **2005**, *433*, 604–607. [CrossRef]

123. Croton, D.J.; Springel, V.; White, S.D.M.; De Lucia, G.; Frenk, C.S.; Gao, L.; Jenkins, A.; Kauffmann, G.; Navarro, J.F.; Yoshida, N. The many lives of active galactic nuclei: Cooling flows, black holes and the luminosities and colours of galaxies. *Mon. Not. RAS* **2006**, *365*, 11–28. [CrossRef]

124. Kelly, B.C.; Merloni, A. Mass Functions of Supermassive Black Holes across Cosmic Time. *Adv. Astron.* **2012**, *2012*, 970858. [CrossRef]

125. Thorne, K.S. Disk-Accretion onto a Black Hole. II. Evolution of the Hole. *Astrophys. J.* **1974**, *191*, 507–520. [CrossRef]

126. King, A.R.; Pringle, J.E.; Hofmann, J.A. The evolution of black hole mass and spin in active galactic nuclei. *Mon. Not. RAS* **2008**, *385*, 1621–1627. [CrossRef]

127. Narayan, R.; Chael, A.; Chatterjee, K.; Ricarte, A.; Curd, B. Jets in Magnetically Arrested Hot Accretion Flows: Geometry, Power and Black Hole Spindown. *arXiv* **2021**, arXiv:2108.12380.

128. Kormendy, J.; Ho, L.C. Coevolution (Or Not) of Supermassive Black Holes and Host Galaxies. *Ann. Rev. Astron. Astrophys.* **2013**, *51*, 511–653. [CrossRef]

129. Pesce, D.W.; Palumbo, D.C.M.; Ricarte, A.; Broderick, A.E.; Johnson, M.D.; Nagar, N.M.; Natarajan, P.; Gómez, J.L. Expectations for Horizon-Scale Supermassive Black Hole Population Studies with the ngEHT. *Galaxies* **2022**, *10*, 109. [CrossRef]

130. Brenneman, L. Measuring Supermassive Black Hole Spins in AGN. *Acta Polytech.* **2013**, *53*, 652. [CrossRef]

131. Ramakrishnan, V.; Nagar, N.; Arratia, V.; Hernández-Yévenes, J.; Pesce, D.W.; Nair, D.G.; Bandyopadhyay, B.; Medina-Porcile, C.; Krichbaum, T.P.; Doeleman, S.; et al. Event Horizon and Environs (ETHER): A Curated Database for EHT and ngEHT Targets and Science. *Galaxies* **2023**, *11*, 15. [CrossRef]

132. Emami, R.; Ricarte, A.; Wong, G.N.; Palumbo, D.; Chang, D.; Doeleman, S.S.; Broaderick, A.; Narayan, R.; Weintroub, J.; Wielgus, M.; et al. Unraveling Twisty Linear Polarization Morphologies in Black Hole Images. *arXiv* **2022**, arXiv:2210.01218.

133. Pesce, D.W.; Palumbo, D.C.M.; Narayan, R.; Blackburn, L.; Doeleman, S.S.; Johnson, M.D.; Ma, C.P.; Nagar, N.M.; Natarajan, P.; Ricarte, A. Toward Determining the Number of Observable Supermassive Black Hole Shadows. *Astrophys. J.* **2021**, *923*, 260. [CrossRef]

134. Merritt, D.; Milosavljević, M. Massive Black Hole Binary Evolution. *Liv. Rev. Relat.* **2005**, *8*, 8. [CrossRef]

135. Begelman, M.C.; Blandford, R.D.; Rees, M.J. Massive black hole binaries in active galactic nuclei. *Nature* **1980**, *287*, 307–309. [CrossRef]
136. Armitage, P.J.; Natarajan, P. Accretion during the Merger of Supermassive Black Holes. *Astrophys. J.* **2002**, *567*, L9. [CrossRef]
137. Milosavljević, M.; Merritt, D. The Final Parsec Problem. In Proceedings of the The Astrophysics of Gravitational Wave Sources, College Park, MA, USA, 24–26 April 2003; Centrella, J.M., Ed.; American Institute of Physics Conference Series; Volume 686, pp. 201–210. [CrossRef]
138. Chael, A.A.; Johnson, M.D.; Narayan, R.; Doeleman, S.S.; Wardle, J.F.C.; Bouman, K.L. High-resolution Linear Polarimetric Imaging for the Event Horizon Telescope. *Astrophys. J.* **2016**, *829*, 11. [CrossRef]
139. Akiyama, K.; Kuramochi, K.; Ikeda, S.; Fish, V.L.; Tazaki, F.; Honma, M.; Doeleman, S.S.; Broderick, A.E.; Dexter, J.; Mościbrodzka, M.; et al. Imaging the Schwarzschild-radius-scale Structure of M87 with the Event Horizon Telescope Using Sparse Modeling. *Astrophys. J.* **2017**, *838*, 1. [CrossRef]
140. Broderick, A.E.; Pesce, D.W.; Tiede, P.; Pu, H.Y.; Gold, R. Hybrid Very Long Baseline Interferometry Imaging and Modeling with THEMIS. *Astrophys. J.* **2020**, *898*, 9. [CrossRef]
141. D'Orazio, D.J.; Loeb, A. Repeated Imaging of Massive Black Hole Binary Orbits with Millimeter Interferometry: Measuring Black Hole Masses and the Hubble Constant. *Astrophys. J.* **2018**, *863*, 185. [CrossRef]
142. Lico, R.; Jorstad, S.G.; Marscher, A.P.; Gómez, J.L.; Liodakis, I.; Dahale, R.; Alberdi, A.; Gold, R.; Traianou, T.; Toscano, T.; et al. Multi-Wavelength and Multi-Messenger Studies Using the Next-Generation Event Horizon Telescope. *Galaxies* **2023**, *11*, 17. [CrossRef]
143. Aartsen, M.G. et al. [IceCube Collaboration]. Neutrino emission from the direction of the blazar TXS 0506+056 prior to the IceCube-170922A alert. *Science* **2018**, *361*, 147–151. [CrossRef]
144. Aartsen, M.G. et al. [IceCube Collaboration]. Multimessenger observations of a flaring blazar coincident with high-energy neutrino IceCube-170922A. *Science* **2018**, *361*, eaat1378. [CrossRef]
145. Plavin, A.; Kovalev, Y.Y.; Kovalev, Y.A.; Troitsky, S. Observational Evidence for the Origin of High-energy Neutrinos in Parsec-scale Nuclei of Radio-bright Active Galaxies. *Astrophys. J.* **2020**, *894*, 101. [CrossRef]
146. Plavin, A.V.; Kovalev, Y.Y.; Kovalev, Y.A.; Troitsky, S.V. Directional Association of TeV to PeV Astrophysical Neutrinos with Radio Blazars. *Astrophys. J.* **2021**, *908*, 157. [CrossRef]
147. Giommi, P.; Padovani, P. Astrophysical Neutrinos and Blazars. *Universe* **2021**, *7*, 492. [CrossRef]
148. Plavin, A.V.; Kovalev, Y.Y.; Kovalev, Y.A.; Troitsky, S.V. Growing evidence for high-energy neutrinos originating in radio blazars. *arXiv* **2023**, arXiv:2211.09631.
149. Kovalev, Y.Y.; Pushkarev, A.B.; Nokhrina, E.E.; Plavin, A.V.; Beskin, V.S.; Chernoglazov, A.V.; Lister, M.L.; Savolainen, T. A transition from parabolic to conical shape as a common effect in nearby AGN jets. *Mon. Not. RAS* **2020**, *495*, 3576–3591. [CrossRef]
150. Marscher, A.P.; Jorstad, S.G.; D'Arcangelo, F.D.; Smith, P.S.; Williams, G.G.; Larionov, V.M.; Oh, H.; Olmstead, A.R.; Aller, M.F.; Aller, H.D.; et al. The inner jet of an active galactic nucleus as revealed by a radio-to-γ-ray outburst. *Nature* **2008**, *452*, 966–969. [CrossRef] [PubMed]
151. Chatterjee, K.; Narayan, R. Flux Eruption Events Drive Angular Momentum Transport in Magnetically Arrested Accretion Flows. *Astrophys. J.* **2022**, *941*, 30. [CrossRef]
152. Ripperda, B.; Liska, M.; Chatterjee, K.; Musoke, G.; Philippov, A.A.; Markoff, S.B.; Tchekhovskoy, A.; Younsi, Z. Black Hole Flares: Ejection of Accreted Magnetic Flux through 3D Plasmoid-mediated Reconnection. *Astrophys. J. Lett.* **2022**, *924*, L32. [CrossRef]
153. Jia, H.; Ripperda, B.; Quataert, E.; White, C.J.; Chatterjee, K.; Philippov, A.; Liska, M. Millimeter Observational Signatures of Flares in Magnetically Arrested Black Hole Accretion Models. *arXiv* **2023**, arXiv:2301.09014.
154. Balbus, S.A.; Hawley, J.F. A Powerful Local Shear Instability in Weakly Magnetized Disks. I. Linear Analysis. *Astrophys. J.* **1991**, *376*, 214. [CrossRef]
155. Balbus, S.A.; Hawley, J.F. Instability, turbulence, and enhanced transport in accretion disks. *Rev. Modern Phys.* **1998**, *70*, 1–53. [CrossRef]
156. Gammie, C.F.; McKinney, J.C.; Tóth, G. HARM: A Numerical Scheme for General Relativistic Magnetohydrodynamics. *Astrophys. J.* **2003**, *589*, 444–457. [CrossRef]
157. Porth, O.; Chatterjee, K.; Narayan, R.; Gammie, C.F.; Mizuno, Y.; Anninos, P.; Baker, J.G.; Bugli, M.; Chan, C.K.; Davelaar, J.; et al. The Event Horizon General Relativistic Magnetohydrodynamic Code Comparison Project. *Astrophys. J. Suppl.* **2019**, *243*, 26. [CrossRef]
158. Narayan, R.; Sądowski, A.; Penna, R.F.; Kulkarni, A.K. GRMHD simulations of magnetized advection-dominated accretion on a non-spinning black hole: role of outflows. *Mon. Not. RAS* **2012**, *426*, 3241–3259. [CrossRef]
159. Narayan, R.; Igumenshchev, I.V.; Abramowicz, M.A. Magnetically Arrested Disk: An Energetically Efficient Accretion Flow. *Publ. ASJ* **2003**, *55*, L69–L72. [CrossRef]
160. Chan, C.K.; Psaltis, D.; Özel, F.; Medeiros, L.; Marrone, D.; Sadowski, A.; Narayan, R. Fast Variability and Millimeter/IR Flares in GRMHD Models of Sgr A* from Strong-field Gravitational Lensing. *Astrophys. J.* **2015**, *812*, 103. [CrossRef]
161. Guan, X.; Gammie, C.F.; Simon, J.B.; Johnson, B.M. Locality of MHD Turbulence in Isothermal Disks. *Astrophys. J.* **2009**, *694*, 1010–1018. [CrossRef]
162. Contopoulos, I.; Nathanail, A.; Sądowski, A.; Kazanas, D.; Narayan, R. Numerical simulations of the Cosmic Battery in accretion flows around astrophysical black holes. *Mon. Not. RAS* **2018**, *473*, 721–727. [CrossRef]

163. Sironi, L.; Spitkovsky, A. Relativistic Reconnection: An Efficient Source of Non-thermal Particles. *Astrophys. J. Lett.* **2014**, *783*, L21. [CrossRef]
164. Rowan, M.E.; Sironi, L.; Narayan, R. Electron and Proton Heating in Transrelativistic Magnetic Reconnection. *Astrophys. J.* **2017**, *850*, 29. [CrossRef]
165. Werner, G.R.; Uzdensky, D.A.; Begelman, M.C.; Cerutti, B.; Nalewajko, K. Non-thermal particle acceleration in collisionless relativistic electron-proton reconnection. *Mon. Not. RAS* **2018**, *473*, 4840–4861. [CrossRef]
166. Ball, D.; Sironi, L.; Özel, F. Electron and Proton Acceleration in Trans-relativistic Magnetic Reconnection: Dependence on Plasma Beta and Magnetization. *Astrophys. J.* **2018**, *862*, 80. [CrossRef]
167. Doeleman, S.S.; Fish, V.L.; Broderick, A.E.; Loeb, A.; Rogers, A.E.E. Detecting Flaring Structures in Sagittarius A* with High-Frequency VLBI. *Astrophys. J.* **2009**, *695*, 59–74. [CrossRef]
168. Ricarte, A.; Palumbo, D.C.M.; Narayan, R.; Roelofs, F.; Emami, R. Observational Signatures of Frame Dragging in Strong Gravity. *Astrophys. J. Lett.* **2022**, *941*, L12. [CrossRef]
169. Blandford, R.; Meier, D.; Readhead, A. Relativistic Jets from Active Galactic Nuclei. *Ann. Rev. Astron. Astrophys.* **2019**, *57*, 467–509. [CrossRef]
170. Salpeter, E.E. Accretion of Interstellar Matter by Massive Objects. *Astrophys. J.* **1964**, *140*, 796–800. [CrossRef]
171. Markoff, S.; Bower, G.C.; Falcke, H. How to hide large-scale outflows: Size constraints on the jets of Sgr A*. *Mon. Not. RAS* **2007**, *379*, 1519–1532. [CrossRef]
172. Yusef-Zadeh, F.; Roberts, D.; Wardle, M.; Heinke, C.O.; Bower, G.C. Flaring Activity of Sagittarius A* at 43 and 22 GHz: Evidence for Expanding Hot Plasma. *Astrophys. J.* **2006**, *650*, 189–194. [CrossRef]
173. Brinkerink, C.; Falcke, H.; Brunthaler, A.; Law, C. Persistent time lags in light curves of Sagittarius A*: evidence of outflow. *arXiv* **2021**, arXiv:2107.13402.
174. Emami, R.; Anantua, R.; Ricarte, A.; Doeleman, S.S.; Broderick, A.; Wong, G.; Blackburn, L.; Wielgus, M.; Narayan, R.; Tremblay, G.; et al. Probing Plasma Composition with the Next Generation Event Horizon Telescope (ngEHT). *Galaxies* **2023**, *11*, 11. [CrossRef]
175. Chael, A.; Narayan, R.; Johnson, M.D. Two-temperature, Magnetically Arrested Disc simulations of the jet from the supermassive black hole in M87. *Mon. Not. RAS* **2019**, *486*, 2873–2895. [CrossRef]
176. Abbott, B.P.; Abbott, R.; Abbott, T.D.; Acernese, F.; Ackley, K.; Adams, C.; Adams, T.; Addesso, P.; Adhikari, R.X.; Adya, V.B.; et al. GW170817: Observation of Gravitational Waves from a Binary Neutron Star Inspiral. *Phys. Rev. Lett.* **2017**, *119*, 161101. [CrossRef]
177. Abbott, B.P.; Abbott, R.; Abbott, T.D.; Acernese, F.; Ackley, K.; Adams, C.; Adams, T.; Addesso, P.; Adhikari, R.X.; Adya, V.B.; et al. Gravitational Waves and Gamma-Rays from a Binary Neutron Star Merger: GW170817 and GRB 170817A. *Astrophys. J. Lett.* **2017**, *848*, L13. [CrossRef]
178. Sari, R.; Piran, T.; Halpern, J.P. Jets in Gamma-Ray Bursts. *Astrophys. J. Lett.* **1999**, *519*, L17–L20. [CrossRef]
179. Mirabel, I.F.; Rodríguez, L.F. Sources of Relativistic Jets in the Galaxy. *Ann. Rev. Astron. Astrophys.* **1999**, *37*, 409–443. [CrossRef]
180. Fender, R. Jets from X-ray binaries. In *Compact Stellar X-ray Sources*; Cambridge University Press: Cambridge, UK, 2006; Volume 39, pp. 381–419.
181. Mooley, K.P.; Deller, A.T.; Gottlieb, O.; Nakar, E.; Hallinan, G.; Bourke, S.; Frail, D.A.; Horesh, A.; Corsi, A.; Hotokezaka, K. Superluminal motion of a relativistic jet in the neutron-star merger GW170817. *Nature* **2018**, *561*, 355–359. [CrossRef] [PubMed]
182. Alexander, K.D.; van Velzen, S.; Horesh, A.; Zauderer, B.A. Radio Properties of Tidal Disruption Events. *Space Sci. Rev.* **2020**, *216*, 81. [CrossRef]
183. Falcke, H.; Körding, E.; Markoff, S. A scheme to unify low-power accreting black holes. Jet-dominated accretion flows and the radio/X-ray correlation. *Astron. Astrophys.* **2004**, *414*, 895–903. .:20031683. [CrossRef]
184. Körding, E.G.; Jester, S.; Fender, R. Accretion states and radio loudness in active galactic nuclei: analogies with X-ray binaries. *Mon. Not. RAS* **2006**, *372*, 1366–1378. [CrossRef]
185. Miller-Jones, J.C.A.; Blundell, K.M.; Rupen, M.P.; Mioduszewski, A.J.; Duffy, P.; Beasley, A.J. Time-sequenced Multi-Radio Frequency Observations of Cygnus X-3 in Flare. *Astrophys. J.* **2004**, *600*, 368–389. [CrossRef]
186. Tetarenko, A.J.; Sivakoff, G.R.; Miller-Jones, J.C.A.; Rosolowsky, E.W.; Petitpas, G.; Gurwell, M.; Wouterloot, J.; Fender, R.; Heinz, S.; Maitra, D.; et al. Extreme jet ejections from the black hole X-ray binary V404 Cygni. *Mon. Not. RAS* **2017**, *469*, 3141–3162. [CrossRef]
187. Tetarenko, A.J.; Sivakoff, G.R.; Miller-Jones, J.C.A.; Bremer, M.; Mooley, K.P.; Fender, R.P.; Rumsey, C.; Bahramian, A.; Altamirano, D.; Heinz, S.; et al. Tracking the variable jets of V404 Cygni during its 2015 outburst. *Mon. Not. RAS* **2019**, *482*, 2950–2972. [CrossRef]
188. Asada, K.; Nakamura, M. The Structure of the M87 Jet: A Transition from Parabolic to Conical Streamlines. *Astrophys. J. Lett.* **2012**, *745*, L28. [CrossRef]
189. Hada, K.; Kino, M.; Doi, A.; Nagai, H.; Honma, M.; Hagiwara, Y.; Giroletti, M.; Giovannini, G.; Kawaguchi, N. The Innermost Collimation Structure of the M87 Jet Down to ~10 Schwarzschild Radii. *Astrophys. J.* **2013**, *775*, 70. [CrossRef]
190. Tseng, C.Y.; Asada, K.; Nakamura, M.; Pu, H.Y.; Algaba, J.C.; Lo, W.P. Structural Transition in the NGC 6251 Jet: an Interplay with the Supermassive Black Hole and Its Host Galaxy. *Astrophys. J.* **2016**, *833*, 288. [CrossRef]
191. Okino, H.; Akiyama, K.; Asada, K.; Gómez, J.L.; Hada, K.; Honma, M.; Krichbaum, T.P.; Kino, M.; Nagai, H.; Bach, U.; et al. Collimation of the Relativistic Jet in the Quasar 3C 273. *Astrophys. J.* **2022**, *940*, 65. [CrossRef]
192. Fender, R.; Woudt, P.A.; Corbel, S.; Coriat, M.; Daigne, F.; Falcke, H.; Girard, J.; Heywood, I.; Horesh, A.; Horrell, J.; et al. ThunderKAT: The MeerKAT Large Survey Project for Image-Plane Radio Transients. In Proceedings of the MeerKAT Science: On the Pathway to the SKA, Stellenbosch, South Africa, 25–27 May 2016; p. 13. [CrossRef]

193. Ho, A.Y.Q.; Phinney, E.S.; Ravi, V.; Kulkarni, S.R.; Petitpas, G.; Emonts, B.; Bhalerao, V.; Blundell, R.; Cenko, S.B.; Dobie, D.; et al. AT2018cow: A Luminous Millimeter Transient. *Astrophys. J.* **2019**, *871*, 73. [CrossRef]

194. Margutti, R.; Metzger, B.D.; Chornock, R.; Vurm, I.; Roth, N.; Grefenstette, B.W.; Savchenko, V.; Cartier, R.; Steiner, J.F.; Terreran, G.; et al. An Embedded X-ray Source Shines through the Aspherical AT 2018cow: Revealing the Inner Workings of the Most Luminous Fast-evolving Optical Transients. *Astrophys. J.* **2019**, *872*, 18. [CrossRef]

195. Curd, B.; Emami, R.; Roelofs, F.; Anantua, R. Modeling Reconstructed Images of Jets Launched by SANE Super-Eddington Accretion Flows around SMBHs with the ngEHT. *Galaxies* **2022**, *10*, 117. [CrossRef]

196. Eubanks, T.M. Anchored in Shadows: Tying the Celestial Reference Frame Directly to Black Hole Event Horizons. *arXiv* **2020**, arXiv:2005.09122.

197. Charlot, P.; Jacobs, C.S.; Gordon, D.; Lambert, S.; de Witt, A.; Böhm, J.; Fey, A.L.; Heinkelmann, R.; Skurikhina, E.; Titov, O.; et al. The third realization of the International Celestial Reference Frame by very long baseline interferometry. *Astron. Astrophys.* **2020**, *644*, A159. [CrossRef]

198. Reid, M.J.; Honma, M. Microarcsecond Radio Astrometry. *Ann. Rev. Astron. Astrophys.* **2014**, *52*, 339–372. [CrossRef]

199. Rioja, M.; Dodson, R. High-precision Astrometric Millimeter Very Long Baseline Interferometry Using a New Method for Atmospheric Calibration. *Astron. J.* **2011**, *141*, 114. [CrossRef]

200. Sokolovsky, K.V.; Kovalev, Y.Y.; Pushkarev, A.B.; Lobanov, A.P. A VLBA survey of the core shift effect in AGN jets. I. Evidence of dominating synchrotron opacity. *Astron. Astrophys.* **2011**, *532*, A38. [CrossRef]

201. Pushkarev, A.B.; Hovatta, T.; Kovalev, Y.Y.; Lister, M.L.; Lobanov, A.P.; Savolainen, T.; Zensus, J.A. MOJAVE: Monitoring of Jets in Active galactic nuclei with VLBA Experiments. IX. Nuclear opacity. *Astron. Astrophys.* **2012**, *545*, A113. [CrossRef]

202. Jiang, W.; Shen, Z.; Martí-Vidal, I.; Wang, X.; Jiang, D.; Kawaguchi, N. Millimeter-VLBI Observations of Low-luminosity Active Galactic Nuclei with Source-frequency Phase Referencing. *Astrophys. J. Lett.* **2021**, *922*, L16. [CrossRef]

203. Kardashev, N.S. Cosmological proper motion. *Astron. Zhurnal* **1986**, *63*, 845–849.

204. Paine, J.; Darling, J.; Graziani, R.; Courtois, H.M. Secular Extragalactic Parallax: Measurement Methods and Predictions for Gaia. *Astrophys. J.* **2020**, *890*, 146. [CrossRef]

205. Hinshaw, G.; Weiland, J.L.; Hill, R.S.; Odegard, N.; Larson, D.; Bennett, C.L.; Dunkley, J.; Gold, B.; Greason, M.R.; Jarosik, N.; et al. Five-Year Wilkinson Microwave Anisotropy Probe Observations: Data Processing, Sky Maps, and Basic Results. *Astrophys. J. Suppl.* **2009**, *180*, 225–245. [CrossRef]

206. Plavin, A.V.; Kovalev, Y.Y.; Pushkarev, A.B.; Lobanov, A.P. Significant core shift variability in parsec-scale jets of active galactic nuclei. *Mon. Not. RAS* **2019**, *485*, 1822–1842. [CrossRef]

207. Riess, A.G.; Casertano, S.; Yuan, W.; Macri, L.M.; Scolnic, D. Large Magellanic Cloud Cepheid Standards Provide a 1% Foundation for the Determination of the Hubble Constant and Stronger Evidence for Physics beyond ΛCDM. *Astrophys. J.* **2019**, *876*, 85. [CrossRef]

208. Aghanim, N. et al. [Planck Collaboration]. Planck 2018 results. VI. Cosmological parameters. *Astron. Astrophys.* **2020**, *641*, A6. [CrossRef]

209. Pesce, D.W.; Braatz, J.A.; Reid, M.J.; Riess, A.G.; Scolnic, D.; Condon, J.J.; Gao, F.; Henkel, C.; Impellizzeri, C.M.V.; Kuo, C.Y.; et al. The Megamaser Cosmology Project. XIII. Combined Hubble Constant Constraints. *Astrophys. J. Lett.* **2020**, *891*, L1. [CrossRef]

210. Wong, K.C.; Suyu, S.H.; Chen, G.C.F.; Rusu, C.E.; Millon, M.; Sluse, D.; Bonvin, V.; Fassnacht, C.D.; Taubenberger, S.; Auger, M.W.; et al. H0LiCOW-XIII. A 2.4 per cent measurement of H_0 from lensed quasars: 5.3σ tension between early- and late-Universe probes. *Mon. Not. RAS* **2020**, *498*, 1420–1439. [CrossRef]

211. Miyoshi, M.; Moran, J.; Herrnstein, J.; Greenhill, L.; Nakai, N.; Diamond, P.; Inoue, M. Evidence for a black hole from high rotation velocities in a sub-parsec region of NGC4258. *Nature* **1995**, *373*, 127–129. [CrossRef]

212. Kuo, C.Y.; Braatz, J.A.; Condon, J.J.; Impellizzeri, C.M.V.; Lo, K.Y.; Zaw, I.; Schenker, M.; Henkel, C.; Reid, M.J.; Greene, J.E. The Megamaser Cosmology Project. III. Accurate Masses of Seven Supermassive Black Holes in Active Galaxies with Circumnuclear Megamaser Disks. *Astrophys. J.* **2011**, *727*, 20. [CrossRef]

213. Herrnstein, J.R. Observations of the Sub-Parsec Maser Disk in NGC 4258. Ph.D. Thesis, Harvard University, Cambridge, MA, USA, 1997.

214. Braatz, J.A.; Reid, M.J.; Humphreys, E.M.L.; Henkel, C.; Condon, J.J.; Lo, K.Y. The Megamaser Cosmology Project. II. The Angular-diameter Distance to UGC 3789. *Astrophys. J.* **2010**, *718*, 657–665. [CrossRef]

215. Reid, M.J.; Braatz, J.A.; Condon, J.J.; Lo, K.Y.; Kuo, C.Y.; Impellizzeri, C.M.V.; Henkel, C. The Megamaser Cosmology Project. IV. A Direct Measurement of the Hubble Constant from UGC 3789. *Astrophys. J.* **2013**, *767*, 154. [CrossRef]

216. Yates, J.A.; Field, D.; Gray, M.D. Non-local radiative transfer for molecules: modelling population inversions in water masers. *Mon. Not. RAS* **1997**, *285*, 303–316. [CrossRef]

217. Gray, M.D.; Baudry, A.; Richards, A.M.S.; Humphreys, E.M.L.; Sobolev, A.M.; Yates, J.A. The physics of water masers observable with ALMA and SOFIA: model predictions for evolved stars. *Mon. Not. RAS* **2016**, *456*, 374–404. [CrossRef]

218. Humphreys, E.M.L.; Greenhill, L.J.; Reid, M.J.; Beuther, H.; Moran, J.M.; Gurwell, M.; Wilner, D.J.; Kondratko, P.T. First Detection of Millimeter/Submillimeter Extragalactic H_2O Maser Emission. *Astrophys. J. Lett.* **2005**, *634*, L133–L136. [CrossRef]

219. Humphreys, E.M.L.; Vlemmings, W.H.T.; Impellizzeri, C.M.V.; Galametz, M.; Olberg, M.; Conway, J.E.; Belitsky, V.; De Breuck, C. Detection of 183 GHz H_2O megamaser emission towards NGC 4945. *Astron. Astrophys.* **2016**, *592*, L13. [CrossRef]

220. Hagiwara, Y.; Miyoshi, M.; Doi, A.; Horiuchi, S. Submillimeter H_2O Maser in Circinus Galaxy—A New Probe for the Circumnuclear Region of Active Galactic Nuclei. *Astrophys. J. Lett.* **2013**, *768*, L38. [CrossRef]
221. Pesce, D.W.; Braatz, J.A.; Impellizzeri, C.M.V. Submillimeter H_2O Megamasers in NGC 4945 and the Circinus Galaxy. *Astrophys. J.* **2016**, *827*, 68. [CrossRef]
222. Hagiwara, Y.; Horiuchi, S.; Doi, A.; Miyoshi, M.; Edwards, P.G. A Search for Submillimeter H_2O Masers in Active Galaxies: The Detection of 321 GHZ H_2O Maser Emission in NGC 4945. *Astrophys. J.* **2016**, *827*, 69. [CrossRef]
223. Hagiwara, Y.; Horiuchi, S.; Imanishi, M.; Edwards, P.G. Second-epoch ALMA Observations of 321 GHz Water Maser Emission in NGC 4945 and the Circinus Galaxy. *Astrophys. J.* **2021**, *923*, 251. [CrossRef]
224. Kim, D.J.; Fish, V. Spectral Line VLBI Studies Using the ngEHT. *Galaxies* **2023**, *11*, 10. [CrossRef]
225. Arras, P.; Frank, P.; Haim, P.; Knollmüller, J.; Leike, R.; Reinecke, M.; Enßlin, T. Variable structures in M87* from space, time and frequency d interferometry. *Nat. Astron.* **2022**, *6*, 259–269. [CrossRef]
226. Fish, V.L.; Johnson, M.D.; Lu, R.S.; Doeleman, S.S.; Bouman, K.L.; Zoran, D.; Freeman, W.T.; Psaltis, D.; Narayan, R.; Pankratius, V.; et al. Imaging an Event Horizon: Mitigation of Scattering toward Sagittarius A*. *Astrophys. J.* **2014**, *795*, 134. [CrossRef]
227. Lu, R.S.; Roelofs, F.; Fish, V.L.; Shiokawa, H.; Doeleman, S.S.; Gammie, C.F.; Falcke, H.; Krichbaum, T.P.; Zensus, J.A. Imaging an Event Horizon: Mitigation of Source Variability of Sagittarius A*. *Astrophys. J.* **2016**, *817*, 173. [CrossRef]
228. Johnson, M.D. Stochastic Optics: A Scattering Mitigation Framework for Radio Interferometric Imaging. *Astrophys. J.* **2016**, *833*, 74. [CrossRef]
229. Akiyama, K.; Ikeda, S.; Pleau, M.; Fish, V.L.; Tazaki, F.; Kuramochi, K.; Broderick, A.E.; Dexter, J.; Mościbrodzka, M.; Gowanlock, M.; et al. Superresolution Full-polarimetric Imaging for Radio Interferometry with Sparse Modeling. *Astron. J.* **2017**, *153*, 159. [CrossRef]
230. Johnson, M.D.; Bouman, K.L.; Blackburn, L.; Chael, A.A.; Rosen, J.; Shiokawa, H.; Roelofs, F.; Akiyama, K.; Fish, V.L.; Doeleman, S.S. Dynamical Imaging with Interferometry. *Astrophys. J.* **2017**, *850*, 172. [CrossRef]
231. Chael, A.A.; Johnson, M.D.; Bouman, K.L.; Blackburn, L.L.; Akiyama, K.; Narayan, R. Interferometric Imaging Directly with Closure Phases and Closure Amplitudes. *Astrophys. J.* **2018**, *857*, 23. [CrossRef]
232. Blackburn, L.; Chan, C.K.; Crew, G.B.; Fish, V.L.; Issaoun, S.; Johnson, M.D.; Wielgus, M.; Akiyama, K.; Barrett, J.; Bouman, K.L.; et al. EHT-HOPS Pipeline for Millimeter VLBI Data Reduction. *Astrophys. J.* **2019**, *882*, 23. [CrossRef]
233. Janssen, M.; Goddi, C.; van Bemmel, I.M.; Kettenis, M.; Small, D.; Liuzzo, E.; Rygl, K.; Martí-Vidal, I.; Blackburn, L.; Wielgus, M.; et al. rPICARD: A CASA-based calibration pipeline for VLBI data. Calibration and imaging of 7 mm VLBA observations of the AGN jet in M 87. *Astron. Astrophys.* **2019**, *626*, A75. [CrossRef]
234. Broderick, A.E.; Gold, R.; Karami, M.; Preciado-López, J.A.; Tiede, P.; Pu, H.Y.; Akiyama, K.; Alberdi, A.; Alef, W.; Asada, K.; et al. THEMIS: A Parameter Estimation Framework for the Event Horizon Telescope. *Astrophys. J.* **2020**, *897*, 139. [CrossRef]
235. Sun, H.; Bouman, K.L. Deep Probabilistic Imaging: Uncertainty Quantification and Multi-modal Solution Characterization for Computational Imaging. *arXiv* **2020**, arXiv:2010.14462.
236. Park, J.; Byun, D.Y.; Asada, K.; Yun, Y. GPCAL: A Generalized Calibration Pipeline for Instrumental Polarization in VLBI Data. *Astrophys. J.* **2021**, *906*, 85. [CrossRef]
237. Pesce, D.W. A D-term Modeling Code (DMC) for Simultaneous Calibration and Full-Stokes Imaging of Very Long Baseline Interferometric Data. *Astron. J.* **2021**, *161*, 178. [CrossRef]
238. Sun, H.; Bouman, K.L.; Tiede, P.; Wang, J.J.; Blunt, S.; Mawet, D. α-deep Probabilistic Inference (α-DPI): Efficient Uncertainty Quantification from Exoplanet Astrometry to Black Hole Feature Extraction. *Astrophys. J.* **2022**, *932*, 99. [CrossRef]
239. Janssen, M.; Radcliffe, J.F.; Wagner, J. Software and Techniques for VLBI Data Processing and Analysis. *Universe* **2022**, *8*, 527. [CrossRef]
240. Hoak, D.; Barrett, J.; Crew, G.; Pfeiffer, V. Progress on the Haystack Observatory Postprocessing System. *Galaxies* **2022**, *10*, 119. [CrossRef]
241. Yu, W.; Romein, J.W.; Dursi, L.J.; Lu, R.S.; Pope, A.; Callanan, G.; Pesce, D.W.; Blackburn, L.; Merry, B.; Srinivasan, R.; et al. Prospects of GPU Tensor Core Correlation for the SMA and the ngEHT. *Galaxies* **2023**, *11*, 13. [CrossRef]
242. Müller, H.; Lobanov, A.P. DoG-HiT: A novel VLBI multiscale imaging approach. *Astron. Astrophys.* **2022**, *666*, A137, [CrossRef]
243. Levis, A.; Srinivasan, P.P.; Chael, A.A.; Ng, R.; Bouman, K.L. Gravitationally Lensed Black Hole Emission Tomography. In Proceedings of the 2022 IEEE/CVF Conference on Computer Vision and Pattern Recognition (CVPR), New Orleans, LA, USA, 21–24 June 2022; pp. 19809–19818. [CrossRef]
244. Abuter, R. et al. [GRAVITY Collaboration]. Detection of orbital motions near the last stable circular orbit of the massive black hole SgrA*. *Astron. Astrophys.* **2018**, *618*, L10. [CrossRef]
245. Liska, M.T.P.; Chatterjee, K.; Issa, D.; Yoon, D.; Kaaz, N.; Tchekhovskoy, A.; van Eijnatten, D.; Musoke, G.; Hesp, C.; Rohoza, V.; et al. H-AMR: A New GPU-accelerated GRMHD Code for Exascale Computing with 3D Adaptive Mesh Refinement and Local Adaptive Time Stepping. *Astrophys. J. Suppl.* **2022**, *263*, 26. [CrossRef]
246. Mościbrodzka, M.; Gammie, C.F. IPOLE-semi-analytic scheme for relativistic polarized radiative transport. *Mon. Not. RAS* **2018**, *475*, 43–54. [CrossRef]
247. Broderick, A.E.; Fish, V.L.; Johnson, M.D.; Rosenfeld, K.; Wang, C.; Doeleman, S.S.; Akiyama, K.; Johannsen, T.; Roy, A.L. Modeling Seven Years of Event Horizon Telescope Observations with Radiatively Inefficient Accretion Flow Models. *Astrophys. J.* **2016**, *820*, 137. [CrossRef]

248. Bouman, K.L.; Johnson, M.D.; Dalca, A.V.; Chael, A.A.; Roelofs, F.; Doeleman, S.S.; Freeman, W.T. Reconstructing Video of Time-Varying Sources from Radio Interferometric Measurements. *IEEE Trans. Comput. Imaging* **2018**, *4*, 512–527. [CrossRef]
249. Swanner, L.A. *Mountains of Controversy: Narrative and the Making of Contested Landscapes in Postwar American Astronomy*; Harvard University: Cambridge, MA, USA, 2013.
250. Salazar, J.A. Multicultural settler colonialism and indigenous struggle in Hawaiʻi: The politics of astronomy on Mauna a Wākea. Ph.D. Thesis, University of Hawaiʻi at Manoa, Honolulu, HI, USA, 2014.
251. Swanner, L. Instruments of science or conquest? Neocolonialism and modern American astronomy. *Hist. Stud. Natl. Sci.* **2017**, *47*, 293–319. [CrossRef]
252. Kahanamoku, S.; Alegado, R.; Kagawa-Viviani, A.; Kamelamela, K.L.; Kamai, B.; Walkowicz, L.M.; Prescod-Weinstein, C.; Reyes, M.A.D.L.; Neilson, H. A Native Hawaiian-led summary of the current impact of constructing the Thirty Meter Telescope on Maunakea. *arXiv* **2020**, arXiv:2001.00970.
253. Alegado, R. Telescope opponents fight the process, not science. *Nature* **2019**, *572*, 7. [CrossRef]
254. Singh, J.A. Informed consent and community engagement in open field research: Lessons for gene drive science. *BMC Med. Ethics* **2019**, *20*, 54. [CrossRef] [PubMed]
255. Watkins, J. Through wary eyes: Indigenous perspectives on archaeology. *Annu. Rev. Anthropol.* **2005**, *34*, 429–449. [CrossRef]
256. Supernant, K.; Warrick, G. Challenges to critical community-based archaeological practice in Canada. *Can. J. Archaeol. J. Can. d'Archéol.* **2014**, *38*, 563–591.
257. Nichols, T. Hidden in Plain Sight Merging the Physics Laboratory with the Surrounding Environment. 2023. *Unpublished manuscript*. Available online: https://www.scientificamerican.com/article/hidden-in-plain-sight/ (accessed on 20 April 2023).
258. Tomblin, D.; Pirtle, Z.; Farooque, M.; Sittenfeld, D.; Mahoney, E.; Worthington, R.; Gano, G.; Gates, M.; Bennett, I.; Kessler, J.; et al. Integrating public deliberation into engineering systems: Participatory technology assessment of NASA's Asteroid Redirect Mission. *Astropolitics* **2017**, *15*, 141–166. [CrossRef]
259. Riordan, M.; Hoddeson, L.; Kolb, A.W. *Tunnel Visions: The Rise and Fall of the Superconducting Super Collider*; University of Chicago Press: Chicago, IL, USA, 2015.
260. Redfield, P. *Space in the Tropics: From Convicts to Rockets in French Guiana*; University of California Press: Auckland City, CA, USA, 2000.
261. Gerrard, M.B. *Whose Backyard, Whose Risk: Fear and Fairness in Toxic and Nuclear Waste Siting*; MIT Press: Cambridge, MA, USA, 1996.
262. Kuletz, V.L. *The Tainted Desert*; Routledge: New York, NY, USA, 1998.
263. Masco, J. The nuclear borderlands. In *The Nuclear Borderlands*; Princeton University Press: Princeton, NJ, USA, 2013.
264. Hamilton, L.; Scowcroft, B.; Ayers, M.; Bailey, V.; Carnesale, A.; Domenici, P.; Eisenhower, S.; Hagel, C.; Lash, J.; Macfarlane, A.; et al. *Blue Ribbon Commission on America's Nuclear Future: Report to the Secretary of Energy*; Blue Ribbon Commission on America's Nuclear Future (BRC): Washington, DC, USA, 2012.
265. Richter, J.; Bernstein, M.J.; Farooque, M. The process to find a process for governance: Nuclear waste management and consent-based siting in the United States. *Energy Res. Soc. Sci.* **2022**, *87*, 102473. [CrossRef]
266. Frigg, R.; Thompson, E.; Werndl, C. Philosophy of climate science part II: Modelling climate change. *Philos. Compass* **2015**, *10*, 965–977. [CrossRef]
267. Winsberg, E. *Philosophy and Climate Science*; Cambridge University Press: Cambridge, UK, 2018.
268. Samek, W.; Montavon, G.; Vedaldi, A.; Hansen, L.K.; Müller, K.R. *Explainable AI: Interpreting, Explaining and Visualizing Deep Learning*; Springer Nature: Berlin/Heidelberg, Germany, 2019; Volume 11700.
269. Zednik, C. Solving the black box problem: A normative framework for explainable artificial intelligence. *Philos. Technol.* **2021**, *34*, 265–288. [CrossRef]
270. Beisbart, C.; Räz, T. Philosophy of science at sea: Clarifying the interpretability of machine learning. *Philos. Compass* **2022**, *17*, e12830. [CrossRef]
271. Kessler, E.A. *Picturing the Cosmos: Hubble Space Telescope Images and the Astronomical Sublime*; University of Minnesota Press: Minneapolis, MN, USA, 2012.
272. Galison, P.; Hevly, B. (Eds.) *Big Science: The Growth of Large-Scale Research*; Stanford University Press: Stanford, CA, USA, 1992.
273. Knorr Cetina, K. *Epistemic Cultures: How the Sciences Make Knowledge*; Harvard University Press: Cambridge, MA, USA, 1999.
274. Sullivan, W.T. *Cosmic Noise: A History of Early Radio Astronomy/Woodruff T. Sullivan, III*; Cambridge University Press: Cambridge, UK; New York, NY, USA, 2009; p. xxxii.
275. Shrum, W.; Chompalov, I.; Genuth, J. Trust, Conflict and Performance in Scientific Collaborations. *Soc. Stud. Sci.* **2001**, *31*, 681–730. [CrossRef]
276. Boyer-Kassem, T.; Mayo-Wilson, C.; Weisberg, M. *Scientific Collaboration and Collective Knowledge*; Oxford University Press: New York, NY, USA, 2017.
277. Collins, H. *Gravity's Kiss: The Detection of Gravitational Waves*; MIT Press: Cambridge, MA, USA, 2017.
278. Nichols, T. Constructing Stillness: Theorization, Discovery, Interrogation, and Negotiation of the Expanded Laboratory of the Laser Interferometer Gravitational-Wave Observatory. Ph.D. Thesis, Harvard University, Harvard, MA, USA, 2022.
279. Boisot, M.; Nordberg, M.; Yami, S.; Nicquevert, B. *Collisions and Collaboration: The Organization of Learning in the ATLAS Experiment at the LHC*; Oxford University Press: Oxford, UK, 2011. [CrossRef]
280. Ritson, S. Creativity and modelling the measurement process of the Higgs self-coupling at the LHC and HL-LHC. *Synthese* **2021**, *199*, 11887–11911. [CrossRef]

281. Sorgner, H. Constructing 'Do-Able'Dissertations in Collaborative Research: Alignment Work and Distinction in Experimental High-Energy Physics Settings. *Sci. Technol. Stud.* **2022**, *35*, 38–57.
282. Merz, M.; Sorgner, H. Organizational Complexity in Big Science: Strategies and Practices. *Synthese* **2022**, *200*, 211. [CrossRef] [PubMed]
283. Jebeile, J. Values and Objectivity in the Intergovernmental Panel on Climate Change. *Soc. Epistemol.* **2020**, *34*, 453–468. . [CrossRef]
284. Smith, R.W.; Hanle, P.A.; Kargon, R.H.; Tatarewicz, J.N. *The Space Telescope. A study of NASA, Science, Technology, and Politics*; Cambridge University Press: Cambridge, MA, USA, 1993.
285. Vertesi, J. *Shaping Science: Organizations, Decisions, and Culture on NASA's Teams*; University of Chicago Press: Chicago, IL, USA, 2020. [CrossRef]
286. Traweek, S. *Beamtimes and Lifetimes: The World of High Energy Physicists*; Harvard University Press: Harvard, MA, USA, 1988.
287. Mellers, B.; Stone, E.; Murray, T.; Minster, A.; Rohrbaugh, N.; Bishop, M.; Chen, E.; Baker, J.; Hou, Y.; Horowitz, M.; et al. Identifying and cultivating superforecasters as a method of improving probabilistic predictions. *Perspect. Psychol. Sci.* **2015**, *10*, 267–281. [CrossRef]
288. Camerer, C.F.; Dreber, A.; Holzmeister, F.; Ho, T.H.; Huber, J.; Johannesson, M.; Kirchler, M.; Nave, G.; Nosek, B.A.; Pfeiffer, T.; et al. Evaluating the replicability of social science experiments in Nature and Science between 2010 and 2015. *Nat. Hum. Behav.* **2018**, *2*, 637–644. [CrossRef] [PubMed]
289. DellaVigna, S.; Pope, D.; Vivalt, E. Predict science to improve science. *Science* **2019**, *366*, 428–429. [CrossRef] [PubMed]
290. Kitcher, P. The Division of Cognitive Labor. *J. Philos.* **1990**, *87*, 5–22. [CrossRef]
291. Kitcher, P. *The Advancement of Science: Science Without Legend, Objectivity Without Illusions*; Oxford University Press: Oxford, UK, 1993.
292. Zollman, K.J.S. The Communication Structure of Epistemic Communities. *Philos. Sci.* **2007**, *74*, 574–587. [CrossRef]
293. Zollman, K.J.S. The Epistemic Benefit of Transient Diversity. *Erkenntnis* **2010**, *72*, 17–35. [CrossRef]
294. Zollman, K.J. Network Epistemology: Communication in Epistemic Communities. *Philos. Compass* **2013**, *8*, 15–27. [CrossRef]
295. Longino, H. The Social Dimensions of Scientific Knowledge. In *The Stanford Encyclopedia of Philosophy*, Summer 2019 ed.; Zalta, E.N., Ed.; Metaphysics Research Lab, Stanford University: Stanford, MA, USA, 2019.
296. Lalli, R.; Howey, R.; Wintergrün, D. The dynamics of collaboration networks and the history of general relativity, 1925–1970. *Scientometrics* **2020**, *122*, 1129–1170. [CrossRef]
297. Lalli, R.; Howey, R.; Wintergrün, D. The Socio-Epistemic Networks of General Relativity, 1925–1970. In *The Renaissance of General Relativity in Context*; Blum, A.S., Lalli, R., Renn, J., Eds.; Einstein Studies; Springer International Publishing: Cham, Switzerland, 2020; pp. 15–84. [CrossRef]
298. Light, R.; Moody, J. *The Oxford Handbook of Social Networks*; Oxford University Press: Oxford, UK, 2021. [CrossRef]
299. Wüthrich, A. Characterizing a Collaboration by Its Communication Structure. *Synthese, unpublish work.*
300. Šešelja, D. Agent-based models of scientific interaction. *Philos. Compass* **2022**, *17*, e12855. [CrossRef]
301. Resnik, D.B. A Proposal for a New System of Credit Allocation in Science. *Sci. Eng. Ethics* **1997**, *3*, 237–243. [CrossRef]
302. Rennie, D.; Yank, V.; Emanuel, L. When Authorship Fails: A Proposal to Make Contributors Accountable. *JAMA* **1997**, *278*, 579–585. [CrossRef] [PubMed]
303. Cronin, B. Hyperauthorship: A postmodern perversion or evidence of a structural shift in scholarly communication practices? *J. Am. Soc. Inf. Sci. Technol.* **2001**, *52*, 558–569. [CrossRef]
304. Galison, P., The Collective Author. *Scientific Authorship: Credit and Intellectual Property in Science*; Galison, P., Biagioli, M., Eds.; Routledge: New York, NY, USA; Oxford, UK, 2003; pp. 325–353.
305. Wray, K.B. Scientific Authorship in the Age of Collaborative Research. *Stud. Hist. Philos. Sci. Part A* **2006**, *37*, 505–514. [CrossRef]
306. McNutt, M.K.; Bradford, M.; Drazen, J.M.; Hanson, B.; Howard, B.; Jamieson, K.H.; Kiermer, V.; Marcus, E.; Pope, B.K.; Schekman, R.; et al. Transparency in authors' contributions and responsibilities to promote integrity in scientific publication. *Proc. Natl. Acad. Sci. USA* **2018**, *115*, 2557–2560. [CrossRef]
307. Bright, L.K.; Dang, H.; Heesen, R. A Role for Judgment Aggregation in Coauthoring Scientific Papers. *Erkenntnis* **2018**, *83*, 231–252. [CrossRef]
308. Heesen, R. Why the Reward Structure of Science Makes Reproducibility Problems Inevitable. *J. Philos.* **2018**, *115*, 661–674. [CrossRef]
309. Dang, H. Epistemology of Scientific Collaborations. Ph.D. Thesis, University of Pittsburgh, Pittsburgh, PA, USA, 2019.
310. Nogrady, B. Hyperauthorship: The publishing challenges for 'big team' science. *Nature* **2023**, *615*, 175–177. [CrossRef]
311. Habgood-Coote, J. What's the Point of Authors? *Br. J. Philos. Sci.* **2021**, *forthcoming*. [CrossRef]